Simultaneous neuronal expression of human amyloid-β and Tau genes drives global phenotypic and multi-omic changes in *C. elegans*

Angelina Holcom[1,2], Matias Fuentealba[1], Renuka Sivapatham[1], Christina D. King[1], Hadley Osman[1], Anna Foulger[1], Dipa Bhaumik[1], Birgit Schilling[1], David Furman[1], Julie K. Andersen[1,3], Gordon J. Lithgow[1,3]

[1]Buck Institute for Research on Aging; Novato, California, 94945 USA

[2]Leonard Davis School of Gerontology, University of Southern California. Los Angeles, California, 90089, USA

[3]Corresponding authors

glithgow@buckinstitute.org

jandersen@buckinstitute.org

Abstract

Alzheimer's disease and Alzheimer's related diseases (ADRD) are a class of prevalent age-related neurodegenerative disorders characterized by the accumulation of amyloid-β (Aβ) plaques and Tau neurofibrillary tangles. The intricate interplay between Aβ and Tau proteins requires further investigation to better understand the precise mechanisms underlying disease pathology. The nematode *Caenorhabditis elegans* (*C. elegans*) serves as an invaluable model organism for studying aging and neurodegenerative diseases.

Here we performed an unbiased systems analysis of a *C. elegans* strain expressing both Aβ and Tau proteins within neurons. Intriguingly, even at an early stage of adulthood, we observed reproductive impairments and mitochondrial dysfunction consistent with substantial disruptions in mRNA transcript abundance, protein solubility, and metabolite levels. Notably, the simultaneous expression of these two neurotoxic proteins exhibited a synergistic effect, leading to accelerated aging in the model organism. Our comprehensive findings shed new light on the intricate relationship between normal aging processes and the etiology of ADRD. Specifically, we demonstrate the alterations to metabolic functions precede age-related neurotoxicity, offering critical insights into potential therapeutic strategies.

Introduction

Alzheimer's disease and Alzheimer's related diseases (ADRD) represent the most prevalent forms of dementia, affecting millions of individuals worldwide[1]. The major risk factor for ADRD is aging. Pathological hallmarks of these disorders include the formation of amyloid-β (Aβ) plaques, neurofibrillary tangles composed of hyperphosphorylated Tau protein, glial cell activation, and impairment of the blood-brain barrier.

The interaction between Aβ and Tau in AD has been closely linked to hypometabolism in the posterior cingulate cortex, which precedes memory decline[2]. Aβ presence accelerates Tau oligomerization, hyperphosphorylation, and propagation[2–4]. In mouse models where co-expression of Aβ and Tau leads to early synapse loss and synergistic effects on defects in mitochondrial function and turnover[2]. Patients with both Aβ and Tau, as determined by cerebrospinal fluid (CSF) analysis and MRI/PET methods, experience an amplified rate of cognitive decline compared to individuals with only Aβ, only Tau, or neither[5].

Extensive research has focused on finding disease-modifying treatments for AD, including α, β, and γ secretase inhibitors, immunotherapy, and inhibitors of Aβ aggregation. However, these approaches have to date not succeeded in halting disease progression[6]. This suggests the need to explore novel therapeutic targets centered around interactions between Aβ and Tau associated with the disease process or systemic changes in relation to metabolic dysfunction.

We proposed to investigate the multi-omic consequences of pan-neuronal, simultaneous expression of human Aβ and Tau in the model organism *C. elegans*. Leveraging the short 20-day lifespan of *C. elegans*, we set out to uncover potential synergistic outcomes of dual toxic protein expression at a multi-omic level. Previous *C. elegans* studies have separately expressed human Aβ in the body muscle or neurons, resulting in a range of phenotypes[7–9]. Similarly, investigations of Tau expression in *C. elegans* have focused on expression of human Tau containing mutations associated with frontotemporal dementia (FTD), a disorder related to AD[10]. These models have each successfully reproduced certain aspects of AD-like phenotypes, including insoluble Tau accumulation, age-related uncoordinated movement, and neurodegeneration[10].

To examine the impact of simultaneous expression of Aβ and Tau, we crossed *C. elegans* strains expressing pan-neuronal Aβ and pan-neuronal Tau. This unique model allowed us to explore the impact of these AD-related proteins on whole-organism protein insolubility, transcriptome dynamics, and metabolomics across different stages of life, including young, middle, and old age. Significantly, this model allowed is to uncover insights into potential early-life effects on reproductive functions and the intricate relationship between normal aging and the development of chronic age-related pathologies.

Methods

C. elegans strains

The transgenic strains utilized in this study include non-transgenic wild-type N2, CK10 (P_{aex-3}::h4R1N Tau V337M; P_{myo-2}::GFP)[11], CL2355(*smg-1*(*cc546);*P_{snb-1}::Aβ$_{1-42}$ + P_{mtl-2}::GFP)[12], and the simultaneous expression strain GL405 (P_{aex-3}::h4R1N Tau V337M; P_{myo-2}::GFP; *smg-1*(*cc546)*;P_{snb-1}::Aβ$_{1-42}$ + P_{mtl-2}::GFP). CL2355 was obtained from the *Caenorhabditis* Genetic Center and CK10 was obtained from the lab of Dr. Brian Kraemer at the University of Washington. N2, CK10, CL2355, GL405 strains are maintained at 15°C due to the *smg-1*(*cc546)* gene, which allows for the temperature-dependent expression of Aβ. Once the worms reached the fourth larval stage (L4), they were shifted to 25°C to induce Aβ expression. Throughout the study, the worms were cultured on nematode growth media (NGM) plates containing *E. coli* OP50 and passaged once a week.

Referenced Name	**Strain name**	**Genotype**	**Growth condition**	**Experiment condition**
WT	N2	wildtype	15°C	25°C & 20°C
Tau	CK10	P_{aex-3}::h4R1N Tau V337M; P_{myo-2}::GFP	15°C	25°C
Aβ	CL2355	*smg-1(cc546)*;P_{snb-1}::Aβ$_{1-42}$ + P_{mtl-2}::GFP	15°C	25°C
Tau;Aβ, Double transgenic, simultaneous expression	GL405	*smg-1*(*cc546)*;P_{snb-1}::Aβ$_{1-42}$ + P_{mtl-2}::GFP x P_{aex-3}::h4R1N Tau V337M; P_{myo-2}::GFP	15°C	25°C

Fertility and fecundity assay

Egg lays were conducted at 15°C for each strain. Once worms develop to the L4 stage, 10 worms were moved to individual small NGM plates and shifted to 25°C. On day 1 of the adult stage, the number of eggs laid was counted to determine fecundity and the number of hatched larvae was counted to determine fertility. The worms were then transferred to fresh NGM plates. The number of eggs laid, and hatched larvae were counted each day until the end of their reproductive cycle. To determine if there were significant differences in fertility and fecundity among the strains, statistical analysis was performed using ordinary one-way ANOVA with Tukey's multiple comparisons test.

Thrashing assay

Following egg lays conducted at 15°C, the worms were allowed to develop to the L4 stage and then transferred to 10 µg/mL FUdR plates, followed by a shift to 25°C. On day 1 of the adult stage, a droplet of S-basal solution was placed on a glass slide, and a single worm was placed into the droplet to acclimate for 30 seconds. Subsequently, the body bends of the worm were counted for another 30 seconds. This process was repeated for

each strain, with 10-20 worms included in each biological replicate. To determine if there were significant differences in the number of body bends between the strains, statistical analysis was performed using ordinary one-way ANOVA with Tukey's multiple comparisons test.

Mitochondrial oxygen consumption rate assay

To evaluate mitochondrial function, a mitochondrial oxygen consumption rate (OCR) assay was performed. Over 200 worms were mass cultured on 100 mm NGM agar plates at 15°C. Age synchronization was achieved by isolating eggs through hypochlorite treatment of gravid adults. Once the worms reached the L4 stage, they were transferred to NGM plates containing 10 µg/mL FUdR and shifted to a temperature of 25°C. Approximately 200 worms were collected on day 1 of the adult stage for further analysis.

An Agilent Seahorse XFe96 Analyzer was utilized to measure the OCR using a previously described protocol[13]. Briefly, for each strain, approximately 20 worms were loaded into each well of a 96-well microtiter plate, with 8 technical replicates per strain. Basal OCR was measured for 5 cycles, where each cycle consisted of 2 minutes of mixing in the well, 4 minutes of waiting, and 2 minutes of OCR measurement in the well.

To determine if there were significant differences in OCR between the strains, statistical analysis was performed using ordinary one-way ANOVA, followed with Tukey's multiple comparisons test.

Lifespan assay

To assess the lifespan of the worms, egg lays were conducted at 15°C. Once the worms reached the L4 stage, approximately 40-60 worms per strain were transferred to NGM plates containing 10 µg/mL FUdR and maintained at a temperature of 25°C. Three replicates were performed for each strain to ensure robustness and reproducibility of the results. The worms were monitored every two days for touched provoked movement. This was achieved by gently poking the worms with a platinum wire and observing their response. The absence of movement upon stimulation was considered an endpoint, indicating mortality.

Statistical analysis was conducted using survival representation (Kaplan-Meier) in GraphPad Prism™ software. Survival curves were generated, and the lifespan of each strain was compared using the Log-rank (Mantel-Cox) test. This analysis allowed for the assessment of significant differences in survival between strains.

3’ Tag RNA-seq

For the 3’ Tag RNA-seq analysis, worms were mass cultured at 15°C, and age-synchronization was achieved by isolating eggs through hypochlorite treatment of gravid adults. Once the worms reached the L4 stage, they were transferred to FUdR NGM plates and maintained at a temperature of 25°C.

Approximately 1000 worms were collected on the first day of the adult stage and stored in a 1.5 mL Eppendorf tube containing 300-500 µL of RNA lysis buffer from the Zymo Research RNA extraction kit. The samples were immediately placed at -80°C for storage. To facilitate RNA extraction, the samples underwent three cycles of freeze-thaw,

alternating between room temperature and -80°C. Subsequently, the samples were incubated on a heat block at 55°C for 0.5-1 hour.

RNA extraction was performed using a Zymo Research RNA extraction kit according to the provided protocol. The protocol included a DNAse treatment step to remove any genomic DNA contamination. The elution step resulted in approximately 40 µL of purified RNA.

The prepared RNA samples were then sent out on dry ice for 3' Tag RNA-Seq analysis. The sequencing was conducted at the DNA Technologies and Expression Analysis Cores at the UC Davis Genome Center, with support from NIH Shared Instrumentation Grant 1S10OD010786-01.

Binarized transcriptomic aging (BiT age) clock calculation

Read counts from the RNA-seq data were transformed into counts per million using edgeR [15]. Using this file and the regression coefficients in https://github.com/Meyer-DH/AgingClock/blob/main/Data/Predictor_Genes.csv we calculated the biological age of each sample from day 1 using the Python script https://github.com/Meyer-DH/AgingClock/blob/main/src/biological_age_prediction.py

Metabolomics

For metabolomic analysis, worms were mass cultured at 15°C and synchronized by isolating eggs using hypochlorite treatment. Upon reaching the L4 stage, the worms were transferred to FUdR 100mm NGM plates at 25°C. At the adult stage day 1,3,5, and 8, approximately 250µl of worms were collected by washing off with S-basal solution and immediately snap freezing [16,17]. These samples were then submitted to Metabolon Inc. (Morrisville, NC, USA) for global metabolic profiling.

Sample preparation was conducted using the automated MicroLab STAR® system from the Hamilton Company. Prior to the extraction process, several recovery standards were added to the samples for quality control purposes. The extracted samples were analyzed using a Waters ACQUITY ultra-performance liquid chromatography (UPLC) system and a Thermo Scientific Q-Exactive high resolution/accurate mass spectrometer equipped with a heated electrospray ionization (HESI-II) source and Orbitrap mass analyzer operating at a mass resolution of 35,000.

Raw data obtained from the analysis was processed by Metabolon's hardware and software. This involved extraction of the data, identification of peaks, and quality control processing. Each metabolite was corrected by registering the medians to a value of one (1.00) and normalizing each data point proportionately. In certain cases, metabolite data was further normalized to total protein levels determined by Bradford assay to account for differences in metabolite levels due to variations in the amount of biological material present in each sample.

A total of 767 biochemical features were identified, including 695 metabolites with known composition and 72 compounds with unknown structural identity. Statistical analysis was performed using two-way ANOVA to identify biochemicals that exhibited significant

differences between experimental groups. Additionally, a false discovery rate (q-value) was estimated to account for multiple comparisons.

Insoluble proteome

For the insoluble proteome analysis, which is based on [18], worms were mass cultured at 15°C and age-synchronized by isolating eggs using hypochlorite treatment of gravid adults. Upon reaching the L4 stage, the worms were transferred to FUdR NGM plates at 25°C. Approximately 3,000 worms at the adult stage day 1,3,5 and 8 were collected in S-basal solution and stored at -80°C.

To extract the insoluble protein fraction, the samples were thawed and vortexed with worm lysis buffer containing 20 mM Tris base (pH 7.4), 100 mM NaCl, 1 mM $MgCl_2$, and EDTA-free protease inhibitor. The lysate was then sonicated for 10 cycles and centrifuged at 3,000 x g for 4 minutes in a cold room. The resulting supernatant, containing the aqueous-soluble protein fraction, was transferred to new 1.5 mL Eppendorf tubes, and the protein concentration was quantified using a BCA assay.

The protein lysate was further processed by centrifuging it for 15 minutes at 20,000 x g in 4ºC. The resulting supernatant was saved as the SDS-soluble fraction. The pellet obtained from this step was washed with 500µl of worm lysis buffer containing 1% SDS and centrifuged at 20,000 x g for 15 minutes. The supernatant was removed, and this washing step was repeated two more times to remove the SDS-soluble fraction. The remaining pellet, known as the 1% SDS-insoluble protein fraction, was resuspended in 60µl of 7% formic acid and vortexed to dissolve the pellet. Subsequently, the sample was sonicated for 30 minutes and dried in a vacuum concentrator for 1 hour to remove the formic acid solution.

The total amount of 1% SDS-insoluble protein, per sample, was prepared for trypsin digestion. Each sample was reduced using 20 mM dithiothreitol in 50 mM triethylammonium bicarbonate buffer (TEAB) at 50°C for 10 min, cooled to room temperature (RT) and held at RT for 10 min, and alkylated using 40 mM iodoacetamide in 50 mM TEAB at RT in the dark for 30 min. Samples were acidified with 12% phosphoric acid to obtain a final concentration of 1.2% phosphoric acid. S-Trap buffer consisting of 90% methanol in 100 mM TEAB at pH ~7.1, was added and samples were loaded onto the S-Trap mini spin columns. The entire sample volume was spun through the S-Trap mini spin columns at 4,000 × g and RT, binding the proteins to the mini spin columns. Subsequently, S-Trap mini spin columns were washed twice with S-Trap buffer at 4,000 × g at RT and placed into clean elution tubes. Samples were incubated for one hour at 47 oC with sequencing grade trypsin (Promega, San Luis Obispo, CA) dissolved in 50 mM TEAB at a 1:25 (w/w) enzyme:protein ratio. Afterwards, trypsin solution was added again at the same ratio, and proteins were digested overnight at 37°C.

Peptides were sequentially eluted from mini S-Trap spin columns with 50 mM TEAB, 0.5% formic acid (FA) in water, and 50% acetonitrile (ACN) in 0.5% FA. After centrifugal evaporation, samples were resuspended in 0.2% FA in water and desalted with C18 Ziptips (MilliporeSigma, Burlington, MA). Desalted peptides were then subjected to an additional round of centrifugal evaporation and re-suspended in 20 µL of 0.2% FA in water and 1 µL of indexed Retention Time Standard (iRT, Biognosys, Schlieren, Switzerland).

Samples were then subjected to mass spectrometric analysis using a high-performance liquid chromatography (HPLC) system combined with a chip-based HPLC system (Eksigent nano-LC) directly connected to a quadrupole time-of-flight mass spectrometer (TripleTOF 5600, a QqTOF instrument) as detailed in a step-by-step protocol by Xie et al [18].

Each sample was acquired in data-dependent acquisition (DDA) mode to build peptide spectral libraries, as described in Xie et al [18]. Data-Independent Acquisition (DIA)/SWATH data was processed in Spectronaut (version 14.10.201222.47784) using DIA. Data extraction parameters were set as dynamic and non-linear iRT calibration with precision iRT was selected. DIA data was matched against an in-house *Caenorhabditis elegans* spectral library that provides quantitative DIA assays for 3,651 *C. elegans* peptides corresponding to 910 protein groups and supplemented with scrambled decoys (library size fraction of 0.01), using dynamic mass tolerances and dynamic extraction windows. DIA/SWATH data was processed for relative quantification comparing peptide peak areas from different days. Identification was performed using 1% precursor and protein q-value. Quantification was based on the peak areas of extracted ion chromatograms (XICs) of 3 – 6 MS2 fragment ions, specifically b- and y-ions, with q-value sparse data filtering and iRT profiling being applied (Supplementary Table 1). For this sample-set, local normalization was not implemented. Differential protein expression analyses for all comparisons were performed using a paired t-test, and p-values were corrected for multiple testing, using the Storey method [19]. Specifically, group wise testing corrections were applied to obtain q-values. Protein groups with at least two unique peptides, q-value ≤ 0.01, and absolute Log2(fold-change) > 0.58 are significantly altered.

Protein-protein interaction network

We extracted 62 proteins with increased abundance (q-value < 0.1) in the insoluble fraction compared to N2 controls at day 1. We loaded this list of proteins into Cytoscape [20] and generated a protein-protein interaction network using the stringApp plugin [21]. Then, we performed enrichment analysis for Biological Processes (Gene ontology), KEGG pathways, and WormBase phenotypes. We colored the nodes of proteins from the top-enriched processes in the network.

Omic analyses

We conducted several omic analyses to gain a comprehensive understanding of the molecular changes associated with the studied conditions. The following approaches were employed:

Enrichment analysis:

For the RNAseq and insoluble proteome data, we performed enrichment analysis using g:Profiler. The custom background used for each specific comparison included all genes or all proteins measured in that particular analysis. The enrichment analysis was carried out with a user threshold of 0.05, and significance was determined using the Benjamini-Hochberg false discovery rate (FDR) correction. Additionally, WormBase Enrichment Analysis was utilized for some of the RNAseq enrichment, applying a q-value threshold of 0.05 and the previously mentioned custom background. Metaboanalyst was utilized for

enrichment analysis of the metabolomics data, employing a custom background consisting of all measured metabolites.

WGCNA (weighted gene co-expression network analysis):

To identify modules of metabolites that exhibited correlated patterns across samples, we employed WGCNA. This analysis involved using the abundance data of metabolites and allowed us to identify groups or modules of metabolites that displayed similar expression profiles, providing insights into potential coordinated metabolic pathways or regulatory mechanisms[22].

Comparison to human frontal cortex:

Upregulated metabolites in the Day 1 Tau;Aβ mutant strain were compared to metabolites upregulated in the frontal cortex of AD subjects vs non-demented control subjects[23].This comparison was made using Deep Venn and this cross-species analysis aimed to identify common molecular signatures and potential similarities between the studied model organism and human AD.

Generation of heatmap and dot plots:

RStudio was utilized to generate heatmaps and dot plots to provide a comprehensive visual overview of observed molecular changes and enriched pathways.

Data Availability

Raw data and complete MS data sets have been uploaded to the Mass Spectrometry Interactive Virtual Environment (MassIVE) repository, developed by the Center for Computational Mass Spectrometry at the University of California San Diego, and can be downloaded using the following link: https://massive.ucsd.edu/ProteoSAFe/private-dataset.jsp?task=e2c3bbad2f214e88bc70ea487d71a3ed (MassIVE ID number: MSV000092031; ProteomeXchange ID: PXD042484. Enter the username and password in the upper right corner of the page: Username: MSV000092031_reviewer; Password: winter

Results

Expression of Aβ and Tau enhances insoluble protein accumulation in young animals.

To investigate the impact of expression of WT human Aβ and 4R1N Tau containing the V337M mutation on protein aggregation, we generated a *C. elegans* strain with simultaneous pan-neuronal expression of both proteins (Fig. 1A). This was achieved by crossing the existing pan-neuronal Aβ strain, CL2355, with the pan-neuronal Tau strain, CK10. This newly generated strain was first used to determine whether the expression of Aβ and Tau leads to the aggregation of other proteins as we had previously observed in *C. elegans* with aging, via induction by other stressors, e.g., iron[24–26]. We collected insoluble proteins from Day 1 adult worms of WT, Tau, Aβ, and Tau;Aβ strains, followed by mass spectrometric analysis (see Supplementary Table 1) using data-independent acquisition[27,28].

Our findings revealed that Aβ expression alone significantly increased the abundance of insoluble proteins compared to WT worms (Supplementary Fig. 1B). Moreover, when comparing the number of insoluble proteins to the WT strain, the Tau;Aβ strain exhibited a greater increase (Fig. 1B).

A comparison of the insoluble proteins in Tau vs WT, Aβ vs WT, and Tau;Aβ vs WT strains demonstrated an overlap among all three AD strains, with the Tau;Aβ expressing strain showing the most substantial alterations (Fig. 1C). Enrichment analysis of the upregulated proteins in the Tau;Aβ strain highlighted the significant involvement of lipid transport in GO biological processes and molecular functions, including four vitellogenin proteins (Fig. 1C).

To gain insights into the functional interactions of the insoluble proteins in the AD strains, we constructed a protein-protein interaction network. This network revealed associations with germ cells and cell physiology, oxidative phosphorylation, and organism development (Fig. 1D).

Notably, the expression of either Tau or Aβ alone led to increased insolubility of lipid transport proteins associated with reproduction, due to the essential role of vitellogenin proteins in providing yolk to eggs within hermaphrodite worms. Perturbation in lipid transport is also observed in human AD, suggesting that even at an early stage of adulthood, the Tau;Aβ expressing strain exhibits specific aspects relevant to AD [29].

Aβ expression drives transcriptomic changes in Tau;Aβ expressing strain in young animals.

To further characterize the WT, Tau, Aβ, and Tau;Aβ expressing strains, we performed 3' Tag RNAseq analysis on day 1 adult worm samples, utilizing the DNA Technologies and Expression Analysis Cores at the University of California Davis Genome Center. Our analysis revealed distinct transcriptomic profiles among the different strains. The Tau expressing strain displayed a transcript profile similar to that of the WT strain. In contrast, the Aβ expressing strain exhibited a significant number of both upregulated and downregulated mRNAs. Notably, the Tau;Aβ expressing strain showed a substantial increase in upregulated mRNAs compared to the WT strain (Fig. 2A).

When comparing the significant downregulated genes in the AD model strains to the WT strain, we observed a high number of downregulated mRNAs in the Aβ expressing strain, while the Tau strain exhibited a relatively low number. The Tau;Aβ expressing strain shared more downregulated mRNAs with the Aβ expressing strain (Fig. 2B). Interestingly, we identified a single gene (coa-3) that was commonly downregulated in all three AD strains.

Comparing the mRNAs with significant increased abundance in all AD strains to the WT strain, we found that the Aβ strain had over 700 upregulated mRNAs, with more than 200 genes showing similar upregulation in the Tau;Aβ expressing strain (Fig. 2C). In contrast, the Tau expressing strain had a minimal number of significantly upregulated genes, and only one gene (Y68A4A.13) was shared among all three AD strains (Fig. 2C). Tissue enrichment analysis of the Tau;Aβ expressing strain's downregulated genes revealed associations with reproduction and germ line functions (Fig. 2D). GO enrichment analysis

of the downregulated genes in the Tau;Aβ expressing strain, compared to the WT strain, showed enrichment for GO terms associated with ribosomes, protein localization to mitochondria, the NADH dehydrogenase complex, and ATP synthesis coupled electron transport (Fig. 2D).

Upregulated genes were found to be expressed in a range of neurons, including interneurons (AVA, AVK), motor neurons (VA, DA neurons), as well as tissues related to reproduction and specific to the male gonad (Fig. 2E). GO enrichment analysis of the upregulated genes in the Tau;Aβ strain, compared to the WT strain, revealed enrichment for GO terms associated with nucleotide binding, modification of peptidyl-serine, and phosphorylation processes (Fig. 2E).

In addition to alterations in upregulated and downregulated mRNAs associated with the expression of Tau and Aβ, we observed changes in a set of genes defined by Meyer and Schumacher, which are used to predict biological age [14]. These genes support the involvement of specific transcription factors, innate immunity, and neuronal signaling in the modulation of aging. This transcriptomic aging clock predicted that the AD strains exhibited an increased transcriptomic age compared to the average WT transcriptomic age (Supplementary Figure 2).

Overall, our analysis of the day 1 adult transcriptome revealed increased upregulation and downregulation of genes associated with reproduction, the nervous system, and RNA biosynthesis in the Tau;Aβ strain. These findings suggest that the expression of Aβ primarily drives the observed transcriptomic changes, which are closely associated with alterations in the insoluble proteome. Both omics analyses demonstrated systemic changes in the Tau;Aβ strain, particularly in relation to reproduction and mitochondrial function.

Synergistic effects of Aβ and Tau expression on metabolites in young animals.

To gain deeper insights into the systemic consequences of expressing human neurotoxic proteins in *C. elegans*, we conducted global metabolomic analysis using day 1 adult worms from the WT, Tau, Aβ, and Tau;Aβ expressing strains. Tau and Aβ strains exhibited relatively minor differences in metabolite changes compared to the WT strain. However, the Tau;Aβ expressing strain displayed extensive alterations in metabolite profiles compared to the WT strain (Fig. 3A), resembling the trend observed in the Aβ expressing strain (Fig. 3B). Notably, the metabolites in the Tau;Aβ strain showed contrasting abundance compared to the WT strain (Fig. 3C).

Further examination of the metabolites altered in the Tau;Aβ expressing strain revealed that they primarily belonged to the categories of lipids and amino acids (Fig. 3D), with involvement in pathways such as long chain polyunsaturated fatty acids and metabolism of leucine, isoleucine, and valine (Fig. 3E). Interestingly, KEGG pathway analysis showed elevated levels of metabolites associated with aminoacyl tRNA biosynthesis in the Tau;Aβ expressing strain (Fig. 3F). Specifically, a majority of the metabolites involved in aminoacyl tRNA biosynthesis were more abundant in the Tau;Aβ expressing strain, while they tended to be less abundant in the individual Aβ and Tau expressing strains, as well as the WT strain. Aminoacyl tRNAs play a crucial role in protein synthesis by providing substrates for the ribosomal translation of messenger RNA [30]. The upregulation of this

pathway in the Tau;Aβ expressing strain may be connected to the observed increase in protein insolubility, as well as the decreased ribonucleotide binding and structural constituent of ribosome observed in the transcriptomic analysis.

In summary, our metabolomic analysis highlighted the synergistic effects of Aβ and Tau expression on the metabolic profiles in young animals. The Tau;Aβ expressing strain exhibited substantial alterations in metabolites, particularly in lipid and amino acid metabolism. Notably, the upregulation of aminoacyl tRNA biosynthesis pathway in the Tau;Aβ expressing strain may provide a link between increased protein insolubility and the transcriptomic changes observed, including decreased ribonucleotide binding and structural constitution of the ribosome.

Increased protein insolubility induced by Tau and Aβ expression in middle-aged animals.

Building upon our observations of increased protein insolubility in the Tau;Aβ expressing strain in young animals, we investigated this molecular phenotype during the aging process. We collected insoluble proteins from Day 3, 5, and 8 adult worms of the WT, Tau, Aβ, and Tau;Aβ expressing strains, followed by mass spectrometric analysis (see Supplementary Table 1). Our findings revealed that the total abundance of insoluble proteins in the WT strain increased with age, consistent with previous reports[18,24,31]. In contrast, the Aβ and Tau;Aβ strains exhibited lower total insoluble protein abundance on day 3 and 5, but displayed an increase on day 8 (Supplementary Fig. 4A). The Tau expressing strain consistently exhibited lower insoluble protein abundance across all ages.

Comparing insoluble proteins significantly elevated on day 3, 5, and 8 in the WT, Tau, Aβ, and Tau;Aβ strains to Day 1, we observed overlaps on day 3, 5 and 8 with day 1 for all four strains (Fig. 4A). On day 5, the Tau strain showed an increase in insoluble proteins compared to day 1. On day 8, the Aβ and Tau;Aβ strains exhibited an increase in insoluble proteins compared day 1. Enrichment analysis revealed an enrichment of ribonucleotide binding and aminoacyl tRNA ligase proteins in the insoluble proteome of the Tau;Aβ expressing strain on day 8 compared to day 1 (Fig. 4B). Similarly, enrichment analysis of the Tau strain on day 5 compared to day 1 highlighted an increase in proteins associated with ribonucleotide binding (Fig. 4C). Enrichment analysis of the Aβ strain on day 8 compared to day 1 revealed an increase in proteins associated with cytoskeleton structure and ribonucleoprotein granules (Fig. 4D). Furthermore, enrichment analysis of the WT strain on day 8 compared to day 1 showed an increase in proteins involved in ion and small molecule binding (Fig. 4E).

Supplementary Figure 4B demonstrates that the insoluble proteome of the Tau;Aβ strain was increased compared to the WT strain on day 3, 5, and 8, in comparison to Tau or Aβ alone. Enrichment analysis of the insoluble proteome on day 3 and day 5 of the Tau;Aβ strain compared to WT highlighted numerous upregulated ribosomal proteins (Supplementary Fig. 4C). When comparing day 3, 5, and 8 of the Tau;Aβ strain to day 1, the insoluble proteins observed on day 3 and 5 were also present on day 8

(Supplementary Fig. 4D). There was an overlap of insoluble proteins on day 1, 3, 5, and 8 of the Tau;Aβ strain compared to WT, with each day also featuring proteins not observed on the other days (Supplementary Fig. 4E).

Overall, the aging insoluble proteome analysis revealed that the Tau;Aβ expressing strain exhibited an early increase in insoluble proteins on day 1 (Fig. 1), which decreased on day 5 and then increased again on day 8. The aging insoluble proteome of the WT, Tau, and Tau;Aβ strains consisted of proteins involved in binding a range of small molecules. Taken in total, our data suggests that the expression of Tau and/or Aβ leads to a complex remodeling of protein insolubility throughout the proteome. The non-linear aging response observed may reflect compensatory mechanisms aimed at preventing or removing insoluble proteins.

Expression of Tau and Aβ disrupts metabolism throughout life.

To gain insights into the metabolic changes associated with aging in the WT, Tau, Aβ, and Tau;Aβ strains, we performed global metabolomic analysis. We observed that significant changes in metabolites were primarily evident on day 8 for the WT and Tau expressing strains (Fig. 5A). The Aβ expressing strain exhibited a slight increase in significantly altered metabolites on day 5, which became more prominent on day 8. In contrast, the Tau;Aβ expressing strain showed the most significant changes on all three days, indicating a potential additive or synergistic relationship resulting from the simultaneous expression of both proteins in neurons.

Comparing the metabolite levels on day 8 compared to day 1 for each strain, we identified an overlap in metabolites altered in abundance on day 8 across all four strains. However, the Tau;Aβ strain had a greater number of unique lower abundance metabolites that did not overlap with the other strains (Supplementary Fig. 5A&B). When comparing the AD strains to the WT on day 3, 5, and 8, the Tau;Aβ strain exhibited the most significant alterations in metabolites on day 5 (Supplementary Fig. 5C).

We performed a weighted correlation network analysis (WGCNA) to cluster highly correlated metabolites into different modules. One of the modules, labeled "salmon," displayed relatively consistent levels of clustered metabolites in the WT and Tau expressing strains (Fig. 5B). The Aβ strain showed a slight increase on day 8, while the Tau;Aβ strain exhibited higher levels on day 1 that decreased with age, reaching WT levels on day 8. Metabolite set enrichment analysis of this module revealed that it primarily consisted of metabolites involved in glycolysis and gluconeogenesis pathways (Fig. 5C). Examining the levels of metabolites within the module, we observed mostly downregulation from day 1 to 8 in the WT and Tau strains, and from day 1 to 5 in the Aβ strain. However, in the Tau;Aβ strain, the metabolites were initially upregulated on day 1 and day 5, followed by a decrease on day 8, reaching levels similar to those in the WT and Tau strains.

In addition to the "salmon" WGCNA module, we also identified a second module labeled "purple", which represents a cluster of metabolites that exhibit an increase on day 1 and decrease with age in the Tau;Aβ strain, while they increase with age in the WT strain (Supplementary Fig.5D&E). These metabolites are associated with α-linolenic acid metabolism and fatty acid biosynthesis pathways (Supplementary Fig.5F).

Elevated pathways in the Tau;Aβ strain, including energy, fat, and mitochondrial function, are consistent with the alterations observed in genes, proteins, and metabolites associated with the mitochondria and lipids in the day 1 transcriptomics, insoluble proteome, and metabolomic analyses. This suggests that the expression of Tau and Aβ leads to disruptions in energy metabolism, fat metabolism, and mitochondrial function, which may contribute to the observed changes in the proteome and metabolome associated with the Tau;Aβ strain.

Tau and Aβ expression in young adult worms resemble WT aging at insoluble proteome and metabolic levels.

Comparing insoluble proteome and metabolomic changes in the day 1 Tau;Aβ expressing strain to the aged WT strain revealed similarities between the two conditions. Proteins that were more abundant in the insoluble proteome of day 8 WT compared to day 1 WT overlapped with the majority of insoluble proteins in day 1 Tau;Aβ compared to day 1 WT. These overlapping proteins were enriched for lipid transport and localization processes (Fig. 6A). Similarly, some of the metabolites that were altered in day 8 WT compared to day 1 WT also overlapped with metabolites altered in day 1 Tau;Aβ compared to day 1 WT (Fig. 6B). In the Tau;Aβ strain, these metabolites were already elevated on day 1, resembling the levels observed in day 8 WT.

By utilizing WGCNA, we discovered a metabolite cluster known as the "midnight blue" module, which displayed an age-dependent increase in WT (Fig. 6C). However, in the Tau;Aβ expressing strain, these metabolites were already elevated on day 1. These metabolites are associated with the plasmalogen synthesis pathway, which showed increased abundance in day 8 WT and day 1-5 Tau;Aβ. Plasmalogens are important for the structure of lipoproteins, synaptic membranes, and ion transport.

This suggests that the expression of Tau and Aβ in young adult worms resembles the aging-associated changes observed in the insoluble proteome and metabolic pathways of WT worms. The simultaneous expression of Tau and Aβ in young adult worms appears to accelerate and enhance aging processes, particularly those affecting lipid pathways. The observed similarities between the insoluble proteome and metabolic changes in the Tau;Aβ strain on day 1 and the aged WT strain suggest that the presence of Tau and Aβ proteins leads to an accelerated aging phenotype, resembling the changes typically seen in older organisms. These alterations in lipid pathways, including lipid transport, localization, and plasmalogen synthesis, may contribute to the

dysregulation of cellular processes and potentially exacerbate the detrimental effects associated with aging.

Systemic phenotypes observed with expression of Tau or Aβ.

With this enhanced aging observed in the Tau;Aβ strain, as indicated by the omic-level changes, we investigated the phenotypic consequences. In the omic data set, we observed changes in proteins, genes and metabolites associated with the mitochondria. This result led us to test mitochondrial function by measuring the worm's ability to move and the rate of oxygen consumption of the mitochondria. Movement patterns of the worms were quantitated by measuring the number of body bends in a given time. The Tau;Aβ strain exhibited a significantly decreased thrashing rate compared to the WT, Tau, and Aβ strains (Fig. 7A). Mitochondrial function was quantitated by measuring the rate of oxygen consumption using a Seahorse XFe96 Analyzer. The Tau and Tau;Aβ strains displayed increased average oxygen consumption rates compared to the WT and Aβ strains, suggesting heightened mitochondrial activity (Fig. 7B). These findings imply that the omic-level alterations observed in the Tau;Aβ strain have functional implications, particularly in mitochondrial activity.

Considering the increased insolubility of vitellogenin protein and the involvement of genes associated with reproduction, the impact on fertility and fecundity was investigated. The number of eggs laid and the number of eggs that hatched were measured over the first 5 days of adulthood. The Tau and Tau;Aβ strains exhibited a decreased average total number of eggs laid, while the Aβ and Tau;Aβ strains showed a significantly decreased average total progeny (Fig. 7C). Additionally, a lifespan assay was performed, revealing that the Tau;Aβ expressing strain had a decreased median and maximum lifespan compared to the other three strains (Fig. 7D). These results indicate that the pan-neuronal expression of Aβ and Tau exerts systemic effects on the worms, with Aβ affecting progeny production, Tau influencing mitochondrial oxygen consumption rate, and the combined expression of both proteins leading to reduced body movement and lifespan. These observations underscore the impact of Tau and Aβ interactions on the phenotypic characteristics of the worms.

Discussion

In this study, a *C. elegans* model of Alzheimer's disease (AD) proteotoxicity was developed by expressing both human Aβ and human 4R1N Tau containing the V337 mutation in neurons. The purpose of generation of this new dual strain was to allow investigation of the combined effect of Aβ and Tau expression on disease progression. Multi-omic analysis was performed, and the results were validated phenotypically.

The insoluble proteome analysis revealed an increase in insoluble proteins associated with lipid transport in the Tau;Aβ strain compared to the WT strain. Furthermore, these vitellogenin lipid transport proteins are associated with reproduction. As the Tau;Aβ strain ages, they also exhibit an increase in insoluble proteins associated with nucleotide and small molecule binding.

Along with alterations on the proteomic level, mRNA abundance was examined to assess any associations between the two data sets. On day 1, significant changes in mRNAs related to reproduction were observed in the Tau;Aβ strain, consistent with the findings in the insoluble proteome analysis. Changes in mRNAs associated with mitochondria were also detected, which correlated with the findings in the insoluble proteome and metabolic profiles of the aged Tau;Aβ strain. Some similarities were found with the transcriptomic data published by Wang et al., including shared upregulated mRNAs and genes associated with protein phosphorylation and the UDP-glucuronosyl transferase[32]. However, differences were observed in downregulated genes, including those involved in ribosome structure, peptide biosynthesis, protein localization to the mitochondrion, and NADH dehydrogenase complex.

Metabolomic analysis revealed increased changes in metabolite levels linked to aminoacyl tRNA biosynthesis in the Tau;Aβ strain on day 1. These early changes in aminoacyl tRNA biosynthesis and the increased aggregation of nucleotide binding proteins may be interconnected, possibly stemming from an increase in amino acids that serve as precursors to aminoacyl tRNAs. The dysfunction of the binding proteins may prevent proper binding, leading to their aggregation with age. This disruption in mRNA translation and protein synthesis has been observed in the initial stages of AD[33]. Furthermore, the increased abundance of amino acids can be attributed to reduced glucose levels, which prompt the utilization of amino acid oxidation as an alternative energy source[34]. Nevertheless, this increase in amino acid oxidation results in increased ammonia levels, potentially leading to neuronal cell death[34]. Consequently, a rise in oxidative stress-related metabolism occurs to eliminate the excess ammonia, leading to an increased abundance of metabolites in the pathways associated with glutathione, methionine, cysteine, S-adenosylmethionine (SAM) and taurine metabolism, as observed in the day 1 Tau;Aβ metabolomics data.

As the worms aged, there was a further increase in metabolite alterations associated with energy and lipid metabolism in the c strain, which are changes observed in AD[35–40]. These findings suggest that the expression of Tau and Aβ leads to disruptions in energy metabolism, lipid metabolism, and mitochondrial function, which may contribute to the observed changes in the proteome, metabolome and phenotypes associated with the Tau;Aβ strain.

Observed omic changes not only had an impact at the molecular level, but also manifested in noticeable phenotypic alterations, including decreased fertility and altered mitochondrial function in the Tau;Aβ strain. Wang et al. also reported a decrease in progeny viability in their double mutant strain, further highlighting the consequences of the dual expression of Tau and Aβ. Moreover, the decrease in body movement observed in the Tau;Aβ strain aligns with the results obtained from another double mutant strain that expressed Aβ and 4R1N Tau without the V337M mutation [41]. These collective findings provide compelling evidence for the intricate relationship between the

expression of Aβ and Tau, and their associated phenotypic outcomes, emphasizing the significance of their interplay in the context of neurodegenerative diseases.

Comparing the insoluble proteome and metabolomic changes between the day 1 Tau;Aβ strain and the aged WT strain revealed striking similarities, implying a convergence of molecular alterations. The overlapping insoluble proteins were predominantly associated with lipid transport and localization processes. The overlapping metabolites were already initially elevated in the day 1 Tau;Aβ strain while they became more abundant with age in the WT strain. These metabolites were associated with the plasmalogen synthesis pathway, which plays a crucial role in the structure of lipoproteins, synaptic membranes, and ion transport. Simultaneous expression of Tau and Aβ in young adult worms appears to expedite and intensify aging processes, particularly those affecting lipid pathways. These disruptions in lipid pathways, encompassing lipid transport, localization, and plasmalogen synthesis, may contribute to the dysregulation of cellular processes and potentially exacerbate the detrimental effects associated with aging.

The Tau;Aβ strain, when combined with the findings from previous studies by Wang et al. and Benbow et al., collectively demonstrates that the expression of both Aβ and Tau leads to neuronal and systemic phenotypes. This integrated model not only enhances our understanding of the individual contributions of Tau and Aβ but also sheds light on their combined effects, offering a comprehensive view of their impact on AD progression from early life. It enables the examination of early systemic changes in AD, and the identification of potential therapeutic targets.

Importantly, the Tau;Aβ strain contributes novel insights into AD by revealing changes at the metabolite and protein levels, complementing the transcriptomic data provided by Wang et al. The observed overlap between the metabolomic data of the Tau;Aβ strain and those from the frontal cortex of humans with AD confirms that this model accurately replicates the omic changes seen in the disease (Supplementary Figure 3). This strengthens its relevance and utility as a model for studying AD pathogenesis.

Acknowledgements

We would like to thank all members of the Lithgow, Andersen, Schilling, and Furman labs. This work was supported by the Larry L. Hillblom Foundation, NIH Shared Instrumentation Grant 1S10OD010786-01, 1S10OD016281-01 (to Buck Institute for the TripleTOF mass spectrometry system), NIA grants RFAG057358 and R01AG029631. This work was also supported by U54AG075932 and P01AI153559 (to Buck Bioinformatics Core). Traineeship supported by NIA T32 AG052374 awarded to AH. The authors thank Dr. Akos Gerencser and former Brand lab members for assistance with the Seahorse XFe96. DeepVenn was used for venn diagrams.

References

1. Rostagno, A. A. Pathogenesis of Alzheimer's Disease. *Int. J. Mol. Sci.* **24**, 107 (2022).
2. Busche, M. A. & Hyman, B. T. Synergy between amyloid-β and tau in Alzheimer's disease. *Nat. Neurosci.* **23**, 1183–1193 (2020).
3. Lee, W. J. *et al.* Regional Aβ-tau interactions promote onset and acceleration of Alzheimer's disease tau spreading. *Neuron* **110**, 1932-1943.e5 (2022).
4. Zhang, H. *et al.* Interaction between Aβ and Tau in the Pathogenesis of Alzheimer's Disease. *Int. J. Biol. Sci.* **17**, 2181–2192 (2021).
5. Pascoal, T. A. *et al.* Synergistic interaction between amyloid and tau predicts the progression to dementia. *Alzheimers Dement.* **13**, 644–653 (2017).
6. Vegh, C. *et al.* A Bird's-Eye View of the Multiple Biochemical Mechanisms that Propel Pathology of Alzheimer's Disease: Recent Advances and Mechanistic Perspectives on How to Halt the Disease Progression Targeting Multiple Pathways. *J. Alzheimers Dis. JAD* **69**, 631–649 (2019).
7. Chen, X., Barclay, J. W., Burgoyne, R. D. & Morgan, A. Using *C. elegans* to discover therapeutic compounds for ageing-associated neurodegenerative diseases. *Chem. Cent. J.* **9**, (2015).
8. Teschendorf, D. & Link, C. D. What have worm models told us about the mechanisms of neuronal dysfunction in human neurodegenerative diseases? *Mol. Neurodegener.* **4**, 38 (2009).
9. Sin, O., Michels, H. & Nollen, E. A. A. Genetic screens in *Caenorhabditis elegans* models for neurodegenerative diseases. *Biochim. Biophys. Acta BBA - Mol. Basis Dis.* **1842**, 1951–1959 (2014).

10. Alexander, A. G., Marfil, V. & Li, C. Use of *Caenorhabditis elegans* as a model to study Alzheimer's disease and other neurodegenerative diseases. *Front. Genet.* **5**, (2014).
11. Kraemer, B. C. *et al.* Neurodegeneration and defective neurotransmission in a *Caenorhabditis elegans* model of tauopathy. *Proc. Natl. Acad. Sci.* **100**, 9980–9985 (2003).
12. Wu, Y. *et al.* Amyloid-β-Induced Pathological Behaviors Are Suppressed by Ginkgo biloba Extract EGb 761 and Ginkgolides in Transgenic *Caenorhabditis elegans*. *J. Neurosci.* **26**, 13102–13113 (2006).
13. Koopman, M. *et al.* A screening-based platform for the assessment of cellular respiration in *Caenorhabditis elegans*. *Nat. Protoc.* **11**, 1798–1816 (2016).
14. Meyer, D. H. & Schumacher, B. BiT age: A transcriptome-based aging clock near the theoretical limit of accuracy. *Aging Cell* **20**, e13320 (2021).
15. Robinson, M. D., McCarthy, D. J. & Smyth, G. K. edgeR: a Bioconductor package for differential expression analysis of digital gene expression data. *Bioinforma. Oxf. Engl.* **26**, 139–140 (2010).
16. Murphy, J. T. *et al.* Simple nutrients bypass the requirement for HLH-30 in coupling lysosomal nutrient sensing to survival. *PLOS Biol.* **17**, e3000245 (2019).
17. Wang, W. *et al.* Comparative Metabolomic Profiling Reveals That Dysregulated Glycolysis Stemming from Lack of Salvage NAD+ Biosynthesis Impairs Reproductive Development in *Caenorhabditis elegans*. *J. Biol. Chem.* **290**, 26163–26179 (2015).

18. Xie, X. *et al.* Quantification of Insoluble Protein Aggregation in *Caenorhabditis elegans* during Aging with a Novel Data-Independent Acquisition Workflow. *J. Vis. Exp. JoVE* 10.3791/61366 (2020) doi:10.3791/61366.
19. Burger, T. Gentle Introduction to the Statistical Foundations of False Discovery Rate in Quantitative Proteomics. *J. Proteome Res.* **17**, 12–22 (2018).
20. Shannon, P. *et al.* Cytoscape: a software environment for integrated models of biomolecular interaction networks. *Genome Res.* **13**, 2498–2504 (2003).
21. Doncheva, N. T., Morris, J. H., Gorodkin, J. & Jensen, L. J. Cytoscape StringApp: Network Analysis and Visualization of Proteomics Data. *J. Proteome Res.* **18**, 623–632 (2019).
22. Langfelder, P. & Horvath, S. WGCNA: an R package for weighted correlation network analysis. *BMC Bioinformatics* **9**, 559 (2008).
23. Paglia, G. *et al.* An unbiased metabolomic investigation of the Alzheimer's disease brain points to a dysregulation of the mitochondrial aspartate metabolism. *J. Proteome Res.* **15**, 608–618 (2016).
24. Reis-Rodrigues, P. *et al.* Proteomic analysis of age-dependent changes in protein solubility identifies genes that modulate lifespan. *Aging Cell* **11**, 120–127 (2012).
25. Klang, I. M. *et al.* Iron promotes protein insolubility and aging in *C. elegans*. *Aging* **6**, 975–991 (2014).
26. Mark, K. A. *et al.* Vitamin D Promotes Protein Homeostasis and Longevity via the Stress Response Pathway Genes SKN-1, IRE-1, and XBP-1. *Cell Rep.* **17**, 1227–1237 (2016).

27. Gillet, L. C. *et al.* Targeted data extraction of the MS/MS spectra generated by data-independent acquisition: a new concept for consistent and accurate proteome analysis. *Mol. Cell. Proteomics MCP* **11**, O111.016717 (2012).
28. Collins, B. C. *et al.* Multi-laboratory assessment of reproducibility, qualitative and quantitative performance of SWATH-mass spectrometry. *Nat. Commun.* **8**, 291 (2017).
29. Kao, Y.-C., Ho, P.-C., Tu, Y.-K., Jou, I.-M. & Tsai, K.-J. Lipids and Alzheimer's Disease. *Int. J. Mol. Sci.* **21**, 1505 (2020).
30. Ibba, M. & Söll, D. The renaissance of aminoacyl-tRNA synthesis. *EMBO Rep.* **2**, 382–387 (2001).
31. Huang, C. *et al.* Intrinsically aggregation-prone proteins form amyloid-like aggregates and contribute to tissue aging in *Caenorhabditis elegans*. *eLife* **8**, e43059 (2019).
32. Wang, C., Saar, V., Leung, K. L., Chen, L. & Wong, G. Human amyloid β peptide and tau co-expression impairs behavior and causes specific gene expression changes in *Caenorhabditis elegans*. *Neurobiol. Dis.* **109**, 88–101 (2018).
33. Ghosh, A. *et al.* Alzheimer's disease-related dysregulation of mRNA translation causes key pathological features with ageing. *Transl. Psychiatry* **10**, 1–18 (2020).
34. Griffin, J. W. D. & Bradshaw, P. C. Amino Acid Catabolism in Alzheimer's Disease Brain: Friend or Foe? *Oxid. Med. Cell. Longev.* **2017**, (2017).
35. Wilson, D. M. *et al.* Hallmarks of neurodegenerative diseases. *Cell* **186**, 693–714 (2023).

36. François, M. *et al.* Multi-Omics, an Integrated Approach to Identify Novel Blood Biomarkers of Alzheimer's Disease. *Metabolites* **12**, 949 (2022).
37. Poddar, M. K., Banerjee, S., Chakraborty, A. & Dutta, D. Metabolic disorder in Alzheimer's disease. *Metab. Brain Dis.* **36**, 781–813 (2021).
38. Chen, Z. & Zhong, C. Decoding Alzheimer's disease from perturbed cerebral glucose metabolism: Implications for diagnostic and therapeutic strategies. *Prog. Neurobiol.* **108**, 21–43 (2013).
39. Patro, S. *et al.* ATP Synthase and Mitochondrial Bioenergetics Dysfunction in Alzheimer's Disease. *Int. J. Mol. Sci.* **22**, 11185 (2021).
40. Olloquequi, J. *et al.* Impact of New Drugs for Therapeutic Intervention in Alzheimer's Disease. *Front. Biosci. Landmark Ed.* **27**, 146 (2022).
41. Benbow, S. J., Strovas, T. J., Darvas, M., Saxton, A. & Kraemer, B. C. Synergistic toxicity between tau and amyloid drives neuronal dysfunction and neurodegeneration in transgenic *C. elegans*. *Hum. Mol. Genet.* **29**, 495–505 (2020).

Figure 1: Expression of Tau and Aβ increase insoluble proteins early in life. (A) Diagram of the cross used to create the dual model simultaneously expressing both human WT Aβ and mutant Tau. The newly generated strain expresses pan-neuronal human WT Aβ and 4R Tau containing the FTDP-17 mutation V337M as well as both pharyngeal and intestinal GFP. (B) Graph of the number of insoluble proteins significantly upregulated in the AD strains compared to WT on day 1 of adulthood. $q \leq 0.05$. (C) Venn diagram of significantly upregulated insoluble proteins in the strains and heatmap of the lipid transport proteins identified by GO analysis. (D) Protein-protein interaction network of insoluble proteins increased in the AD mutant strains compared to WT. 3 biological replicates, $q \leq 0.1$.

Figure 2: Aβ expression drives transcriptomic changes in the dual Tau;Aβ strain. (A) Volcano plots of fold gene expression change in Tau compared to WT, Aβ compared to WT and Tau;Aβ compared to WT on day 1 of adulthood. (B) Venn diagram of significant genes downregulated and (C) upregulated in Tau, Aβ and Tau;Aβ compared to WT on day 1 of adulthood. (D) Wormbase tissue enrichment and GO enrichment of the genes downregulated in day 1 Tau;Aβ strain compared to WT. (E) Wormbase tissue enrichment and GO enrichment of the genes upregulated in day 1 Tau;Aβ strain compared to WT.

Figure 3: Expression of Tau and Aβ synergistically alters metabolite levels. (A) Bar graph of fold metabolite change in Tau, Aβ and Tau;Aβ compared to WT. (B) Pearson's product-moment correlation of fold metabolite change between Aβ vs WT and Tau vs WT, Tau;Aβ vs WT and Aβ vs WT, and Tau;Aβ vs WT and Tau vs WT. (C) Heatmap of metabolites significantly downregulated and upregulated in Tau;Aβ compared to WT, Tau and Aβ. (D) Graph of super pathways of the Tau;Aβ vs WT metabolites. (E) Graph of subpathways of the Tau;Aβ vs WT metabolites. (F) Heatmap of the metabolites in the aminoacyl tRNA biosynthesis pathway identified by KEGG analysis for all 4 strains.

Figure 4: Expression of Tau and Aβ increases day 8 insoluble proteome.

(A) Graph of the sum of total insoluble protein abundance measured for each strain on day 3, 5, 8 adulthood. (B) Venn diagram of significantly upregulated insoluble proteins in the strains on day 3 compared to day 1, day 5 compared to day 1, and day 8 compared to day 1 for all 4 strains. (C) GO molecular function of proteins upregulated in day 8 vs day 1 in Tau;Aβ. (D) GO molecular function of proteins upregulated in day 5 vs day 1 Tau. (E) Wormbase Gene ontology enrichment of proteins upregulated in day 8 vs day 1 in Aβ. (F) GO molecular function of proteins upregulated in day 8 vs day 1 in WT.

Figure 5: Expression of Tau and Aβ enhances metabolic changes with age. (A) Graph of number of metabolites significantly changing in day 3, day 5 and day 8 vs day 1 in all 4 strains. (B) WGCNA plot of salmon module with all 4 strains from day 1 to day 8. (C) Metabolite set enrichment analysis of metabolites in salmon module. (D) Heatmap of metabolites in salmon module for all strains on day 1, 3, 5 and 8.

Figure 6: Tau and Aβ expression in young adult worms resembles WT aging at insoluble proteome and metabolomic levels. (A) Venn diagram of upregulated insoluble proteins in day 1 Tau;Aβ vs day 1 WT compared to day 8 WT vs day 1 WT and

GO biological process of the insoluble proteins shared between the day 8 WT and day 1 Tau;Aβ. (B) Venn diagram of the metabolites in day 1 Tau;Aβ vs day 1 WT compared to day 8 WT vs day 1 WT and a heatmap of the shared metabolites. (C) WGCNA plot of midnight blue module with all 4 strains from day 1 to day 8 and heatmap of the metabolites in the midnight blue module for all strains on day 1, 3, 5 and 8.

Figure 7: Systemic phenotypes observed in the context of expression of Tau and Aβ. (A) The average total number of eggs laid in the 4 strains. Error bars represent mean ± SEM. (B) The total progeny in the 4 strains. Error bars represent mean ± SEM. (C) The percent of progeny viable was determined by the total number of progeny hatched and total eggs laid. Ordinary one-way ANOVA with Tukey's multiple comparisons test. Error bars represent mean ± SEM. (D) Average thrashing rates of the 4 strains on day 1 of adulthood. Error bars represent mean ± SEM. (E) Average basal mitochondrial oxygen consumption rate (OCR) of day 1 adult WT, Tau, Aβ and Tau;Aβ strains. Error bars represent mean ± SEM. (F) Average lifespan for WT, Tau, Aβ and Tau;Aβ strains. Includes table of average max and median lifespan and log-rank test p-value of AD strains compared to WT. Error bars represent mean ± SEM.

Supplementary Figure 1: Increased upregulated insoluble proteome with Aβ expression. (A) List of insoluble proteins upregulated in Tau vs WT, Aβ vs WT and Tau;Aβ vs WT, significance was based on q ≤0.05. (B) Graph of the sum of total insoluble protein abundance measured for each strain on Day 1 adulthood.

Supplementary Figure 2: Altered predicted biological age of AD strains. (A) Based on transcriptomic aging clock from [14], the predicted biological age of Tau, Aβ and Tau;Aβ are increased compared to WT.

Supplementary Figure 3: Overlap of upregulated metabolites in young Tau;Aβ and in the frontal cortex of individuals with AD. (A) Comparison of upregulated metabolites in the Day 1 Tau;Aβ vs WT to metabolites upregulated in frontal cortex of AD subjects vs non-demented control subjects [23]. The overlap consists of AMP, GMP, S-adenosylmethioninamine, methionine, serine, and tryptophan.

Supplementary Figure 4: Alterations in aged insoluble proteome with enrichment for ribosomal proteins in Tau;Aβ strain. (A) Graph of the sum of total insoluble protein abundance measured for each strain on day 3, 5, 8 adulthood. (B) Venn diagrams of upregulated insoluble proteins on day 3, 5 and 8 of adulthood in Tau, Aβ, and Tau;Aβ compared to WT, significance was based on q ≤0.05. (C) Table of g:Profiler enrichment of day 3 Tau;Aβ vs WT and day 5 Tau;Aβ vs WT. (D) Venn diagram of upregulated insoluble proteins on day 3, 5 and 8 of adulthood in Tau;Aβ compared to day 1 Tau;Aβ, significance was based on q ≤0.05. (E) Venn diagram of upregulated insoluble proteins on day 1, 3, 5 and 8 of adulthood in Tau;Aβ compared to WT, significance was based on q ≤0.05.

Supplementary Figure 5: Enhanced Age-Related Metabolomic Changes in Tau;Aβ, with a Focus on Alpha Linolenic Acid and Fatty Acid Biosynthesis. (A) Venn diagram of downregulated metabolites on day 8 of adulthood in Tau, Aβ, and Tau;Aβ compared to day 1, significance was based on q ≤0.05. (B) Venn diagram of

upregulated metabolites on day 8 of adulthood in Tau, Aβ, and Tau;Aβ compared to day 1, significance was based on q ≤0.05. (C) Table of number of significantly up and down regulated metabolites on day 3, 5 and 8 of adulthood in Tau, Aβ, and Tau;Aβ compared to WT, significance was based on q ≤0.05. (D) WGCNA plot of purple module with all 4 strains from day 1 to day 8. (E) Heatmap of metabolites in purple module for all strains on day 1, 3, 5 and 8. (F) Metabolite set enrichment analysis of metabolites in purple module.

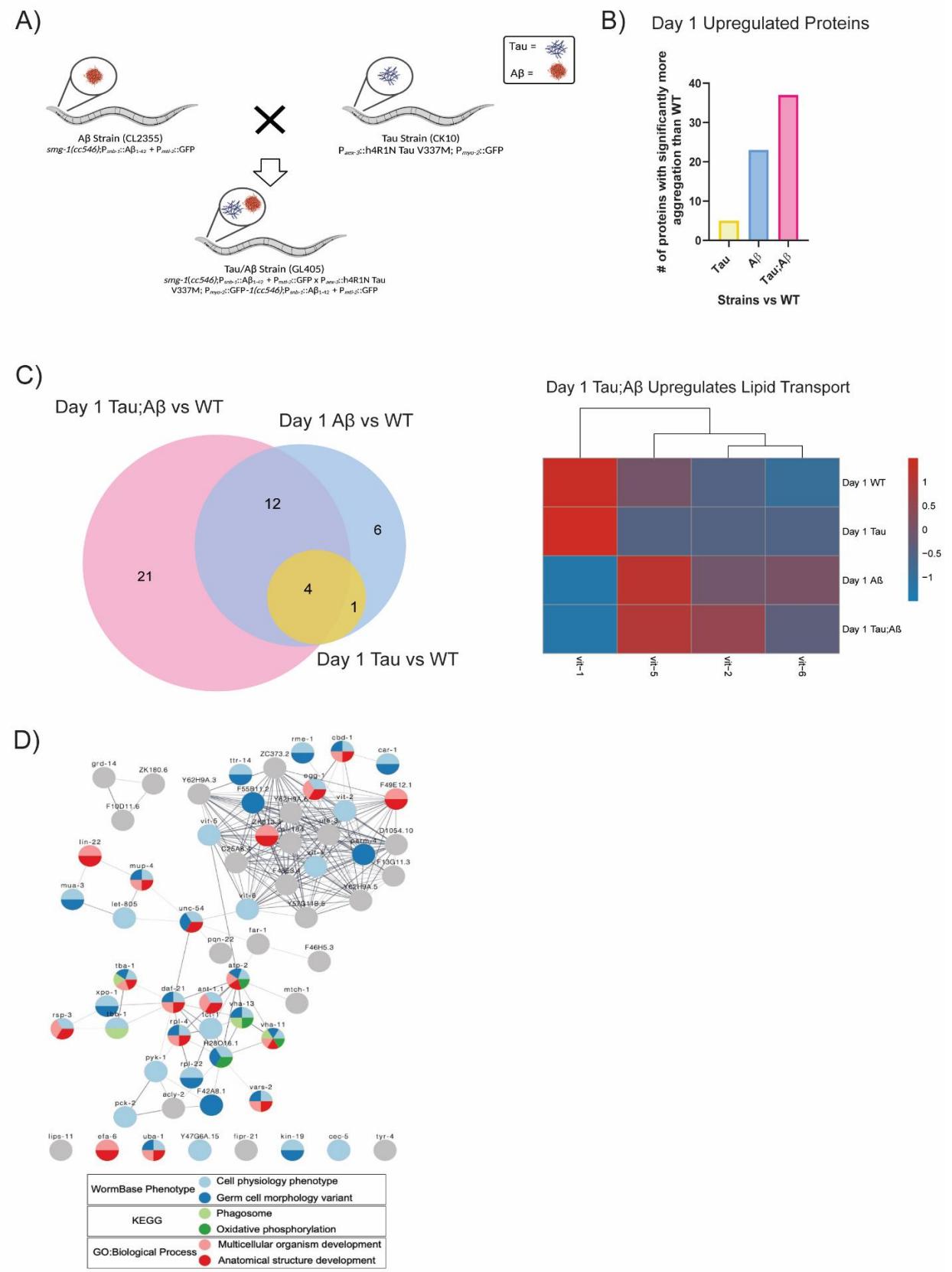
A)
Tau =
Aβ =
Aβ Strain (CL2355)
smg-1(cc546);Pmub-3::Aβ1-42 + Pmtl-2::GFP
Tau Strain (CK10)
Paex-3::h4R1N Tau V337M; Pmyo-2::GFP
Tau/Aβ Strain (GL405)
smg-1(cc546);Pmub-3::Aβ1-42 + Pmtl-2::GFP x Paex-3::h4R1N Tau V337M; Pmyo-2::GFP-1(cc546);Pmub-3::Aβ1-42 + Pmtl-2::GFP
B)
Day 1 Upregulated Proteins
# of proteins with significantly more aggregation than WT
40
30
20
10
0
Tau
Aβ
Tau;Aβ
Strains vs WT
C)
Day 1 Tau;Aβ vs WT
Day 1 Aβ vs WT
Day 1 Tau vs WT
12
6
21
4
1
Day 1 Tau;Aβ Upregulates Lipid Transport
Day 1 WT
Day 1 Tau
Day 1 Aß
Day 1 Tau;Aß
1
0.5
0
−0.5
−1
vit-1
vit-5
vit-2
vit-6
D)
WormBase Phenotype
Cell physiology phenotype
Germ cell morphology variant
KEGG
Phagosome
Oxidative phosphorylation
GO:Biological Process
Multicellular organism development
Anatomical structure development

Figure 1

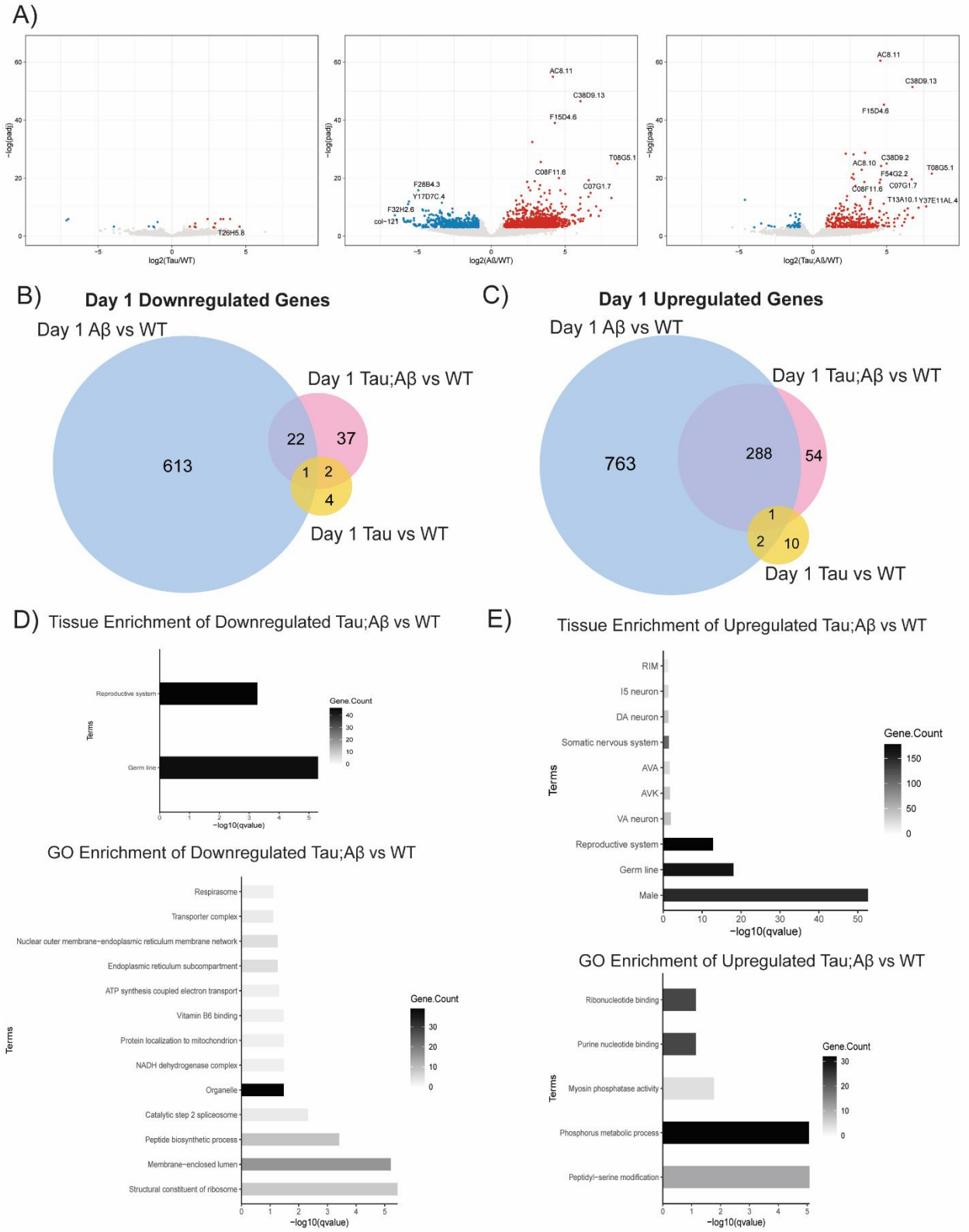
A)
−log(padj)
log2(Tau/WT)
log2(Aß/WT)
log2(Tau;Aß/WT)
T26H5.8
AC8.11
C38D9.13
F15D4.6
T08G5.1
C08F11.6
C07G1.7
F28B4.3
Y17D7C.4
F32H2.6
col−121
AC8.10
C38D9.2
F54G2.2
T13A10.1
Y37E11AL.4
B) Day 1 Downregulated Genes
Day 1 Aβ vs WT
Day 1 Tau;Aβ vs WT
Day 1 Tau vs WT
613
22
37
1
2
4
C) Day 1 Upregulated Genes
Day 1 Aβ vs WT
Day 1 Tau;Aβ vs WT
Day 1 Tau vs WT
763
288
54
1
2
10
D) Tissue Enrichment of Downregulated Tau;Aβ vs WT
Reproductive system
Germ line
Terms
Gene.Count
−log10(qvalue)
GO Enrichment of Downregulated Tau;Aβ vs WT
Respirasome
Transporter complex
Nuclear outer membrane−endoplasmic reticulum membrane network
Endoplasmic reticulum subcompartment
ATP synthesis coupled electron transport
Vitamin B6 binding
Protein localization to mitochondrion
NADH dehydrogenase complex
Organelle
Catalytic step 2 spliceosome
Peptide biosynthetic process
Membrane−enclosed lumen
Structural constituent of ribosome
E) Tissue Enrichment of Upregulated Tau;Aβ vs WT
RIM
I5 neuron
DA neuron
Somatic nervous system
AVA
AVK
VA neuron
Reproductive system
Germ line
Male
GO Enrichment of Upregulated Tau;Aβ vs WT
Ribonucleotide binding
Purine nucleotide binding
Myosin phosphatase activity
Phosphorus metabolic process
Peptidyl−serine modification

Figure 2

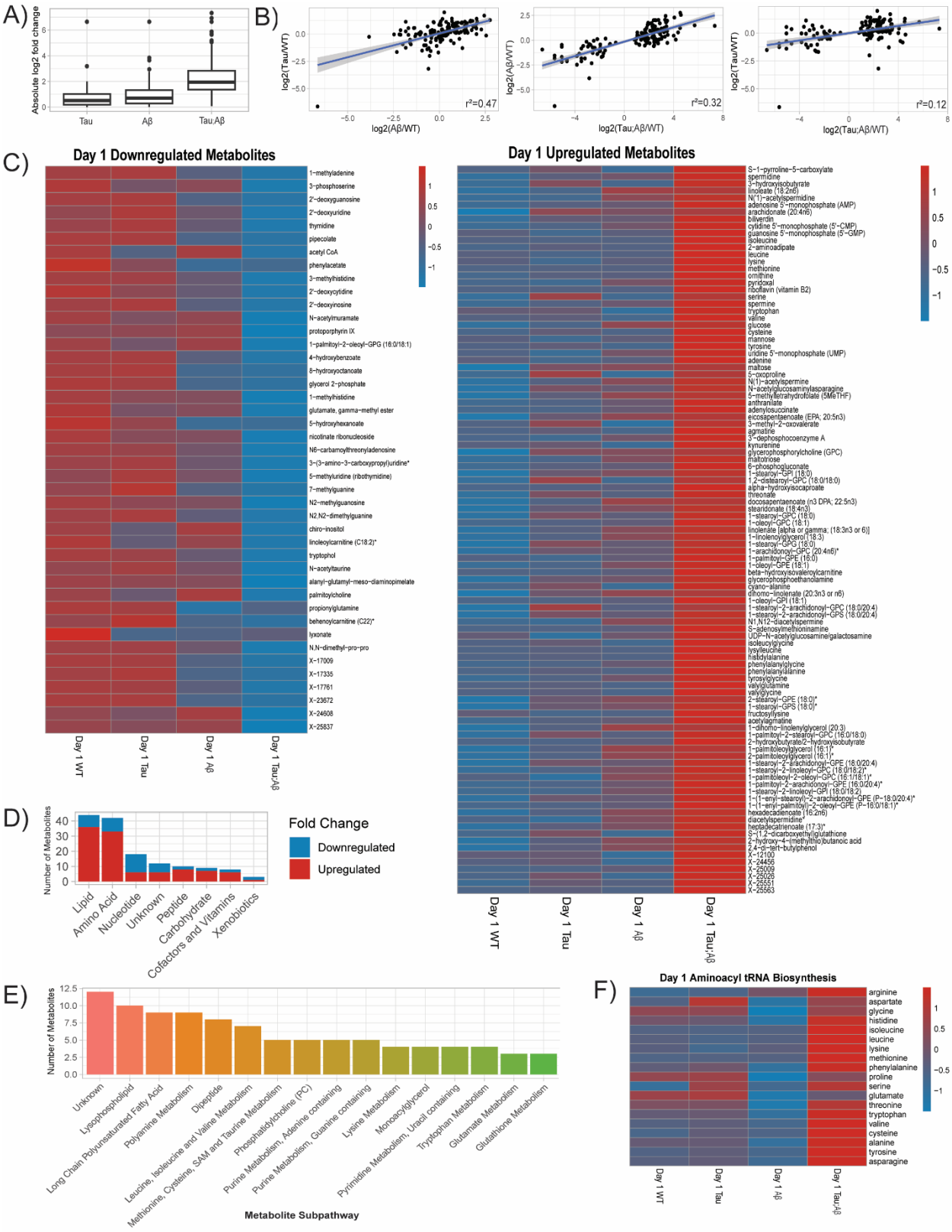
A)
Absolute log2 fold change
Tau
Aβ
Tau:Aβ
B)
log2(Tau/WT)
log2(Aβ/WT)
r²=0.47
log2(Aβ/WT)
log2(Tau;Aβ/WT)
r²=0.32
log2(Tau/WT)
log2(Tau;Aβ/WT)
r²=0.12
C)
Day 1 Downregulated Metabolites
Day 1 Upregulated Metabolites
Day 1 WT
Day 1 Tau
Day 1 Aβ
Day 1 Tau;Aβ
D)
Number of Metabolites
Lipid
Amino Acid
Nucleotide
Unknown
Peptide
Carbohydrate
Cofactors and Vitamins
Xenobiotics
Fold Change
Downregulated
Upregulated
E)
Number of Metabolites
Unknown
Lysophospholipid
Long Chain Polyunsaturated Fatty Acid
Polyamine Metabolism
Dipeptide
Leucine, Isoleucine and Valine Metabolism
Methionine, Cysteine, SAM and Taurine Metabolism
Phosphatidylcholine (PC)
Purine Metabolism, Adenine containing
Purine Metabolism, Guanine containing
Lysine Metabolism
Monoacylglycerol
Pyrimidine Metabolism, Uracil containing
Tryptophan Metabolism
Glutamate Metabolism
Glutathione Metabolism
Metabolite Subpathway
F)
Day 1 Aminoacyl tRNA Biosynthesis
arginine
aspartate
glycine
histidine
isoleucine
leucine
lysine
methionine
phenylalanine
proline
serine
glutamate
threonine
tryptophan
valine
cysteine
alanine
tyrosine
asparagine
Day 1 WT
Day 1 Tau
Day 1 Aβ
Day 1 Tau;Aβ

Figure 3

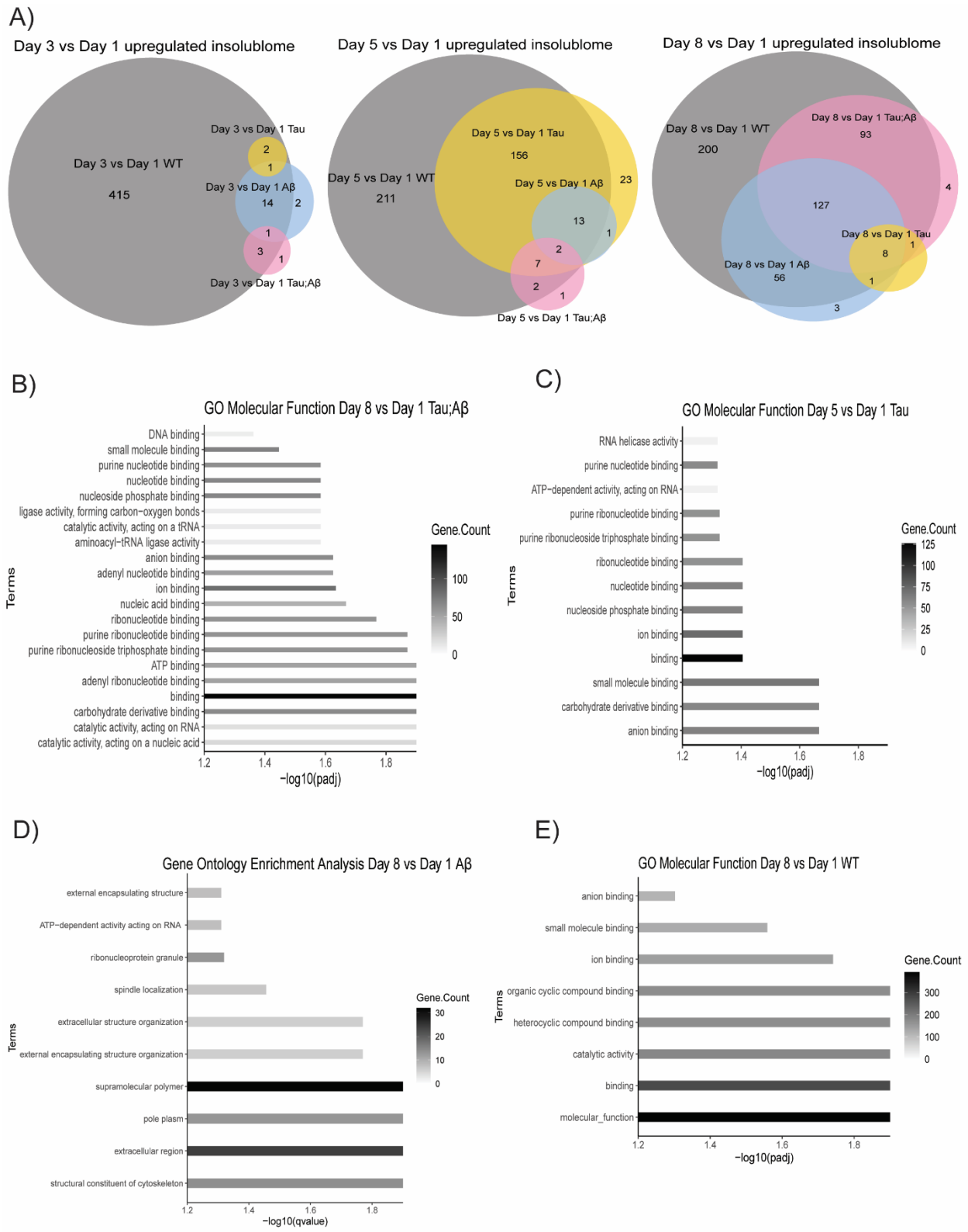
A)
Day 3 vs Day 1 upregulated insolublome
Day 3 vs Day 1 WT
415
Day 3 vs Day 1 Tau
2
1
Day 3 vs Day 1 Aβ
14
2
1
3
1
Day 3 vs Day 1 Tau;Aβ
Day 5 vs Day 1 upregulated insolublome
Day 5 vs Day 1 WT
211
Day 5 vs Day 1 Tau
156
Day 5 vs Day 1 Aβ
23
13
1
2
7
2
1
Day 5 vs Day 1 Tau;Aβ
Day 8 vs Day 1 upregulated insolublome
Day 8 vs Day 1 WT
200
Day 8 vs Day 1 Tau;Aβ
93
4
127
Day 8 vs Day 1 Tau
1
8
Day 8 vs Day 1 Aβ
56
1
3
B)
GO Molecular Function Day 8 vs Day 1 Tau;Aβ
DNA binding
small molecule binding
purine nucleotide binding
nucleotide binding
nucleoside phosphate binding
ligase activity, forming carbon−oxygen bonds
catalytic activity, acting on a tRNA
aminoacyl−tRNA ligase activity
anion binding
adenyl nucleotide binding
ion binding
nucleic acid binding
ribonucleotide binding
purine ribonucleotide binding
purine ribonucleoside triphosphate binding
ATP binding
adenyl ribonucleotide binding
binding
carbohydrate derivative binding
catalytic activity, acting on RNA
catalytic activity, acting on a nucleic acid
Terms
Gene.Count
100
50
0
1.2
1.4
1.6
1.8
−log10(padj)
C)
GO Molecular Function Day 5 vs Day 1 Tau
RNA helicase activity
purine nucleotide binding
ATP−dependent activity, acting on RNA
purine ribonucleotide binding
purine ribonucleoside triphosphate binding
ribonucleotide binding
nucleotide binding
nucleoside phosphate binding
ion binding
binding
small molecule binding
carbohydrate derivative binding
anion binding
Terms
Gene.Count
125
100
75
50
25
0
1.2
1.4
1.6
1.8
−log10(padj)
D)
Gene Ontology Enrichment Analysis Day 8 vs Day 1 Aβ
external encapsulating structure
ATP−dependent activity acting on RNA
ribonucleoprotein granule
spindle localization
extracellular structure organization
external encapsulating structure organization
supramolecular polymer
pole plasm
extracellular region
structural constituent of cytoskeleton
Terms
Gene.Count
30
20
10
0
1.2
1.4
1.6
1.8
−log10(qvalue)
E)
GO Molecular Function Day 8 vs Day 1 WT
anion binding
small molecule binding
ion binding
organic cyclic compound binding
heterocyclic compound binding
catalytic activity
binding
molecular_function
Terms
Gene.Count
300
200
100
0
1.2
1.4
1.6
1.8
−log10(padj)

Figure 4

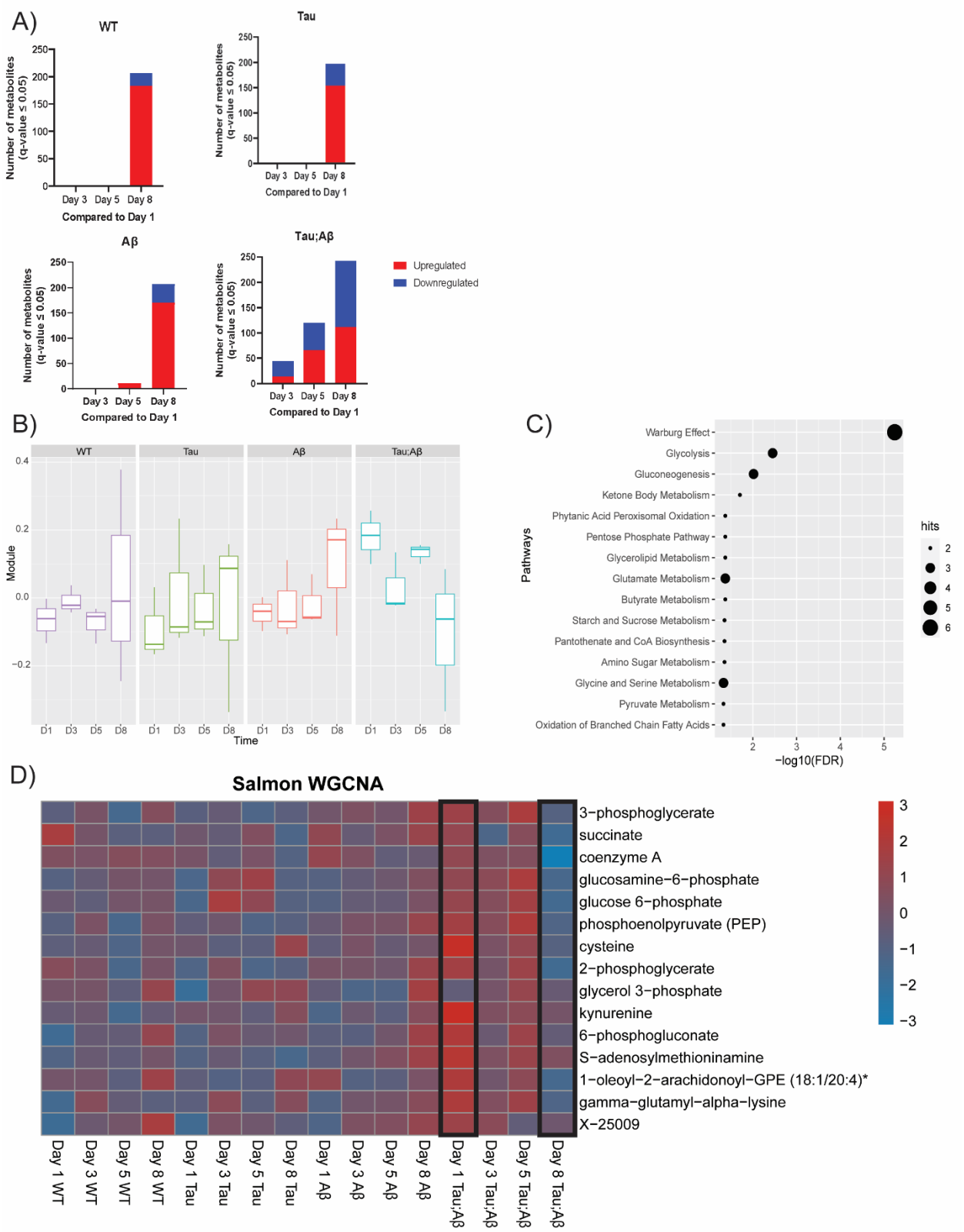
A)
WT
Tau
Aβ
Tau;Aβ
Number of metabolites (q-value ≤ 0.05)
Day 3
Day 5
Day 8
Compared to Day 1
Upregulated
Downregulated
B)
WT
Tau
Aβ
Tau;Aβ
Module
Time
C)
Warburg Effect
Glycolysis
Gluconeogenesis
Ketone Body Metabolism
Phytanic Acid Peroxisomal Oxidation
Pentose Phosphate Pathway
Glycerolipid Metabolism
Glutamate Metabolism
Butyrate Metabolism
Starch and Sucrose Metabolism
Pantothenate and CoA Biosynthesis
Amino Sugar Metabolism
Glycine and Serine Metabolism
Pyruvate Metabolism
Oxidation of Branched Chain Fatty Acids
Pathways
hits
−log10(FDR)
D)
Salmon WGCNA
3−phosphoglycerate
succinate
coenzyme A
glucosamine−6−phosphate
glucose 6−phosphate
phosphoenolpyruvate (PEP)
cysteine
2−phosphoglycerate
glycerol 3−phosphate
kynurenine
6−phosphogluconate
S−adenosylmethioninamine
1−oleoyl−2−arachidonoyl−GPE (18:1/20:4)*
gamma−glutamyl−alpha−lysine
X−25009
Day 1 WT
Day 3 WT
Day 5 WT
Day 8 WT
Day 1 Tau
Day 3 Tau
Day 5 Tau
Day 8 Tau
Day 1 Aβ
Day 3 Aβ
Day 5 Aβ
Day 8 Aβ
Day 1 Tau;Aβ
Day 3 Tau;Aβ
Day 5 Tau;Aβ
Day 8 Tau;Aβ

Figure 5

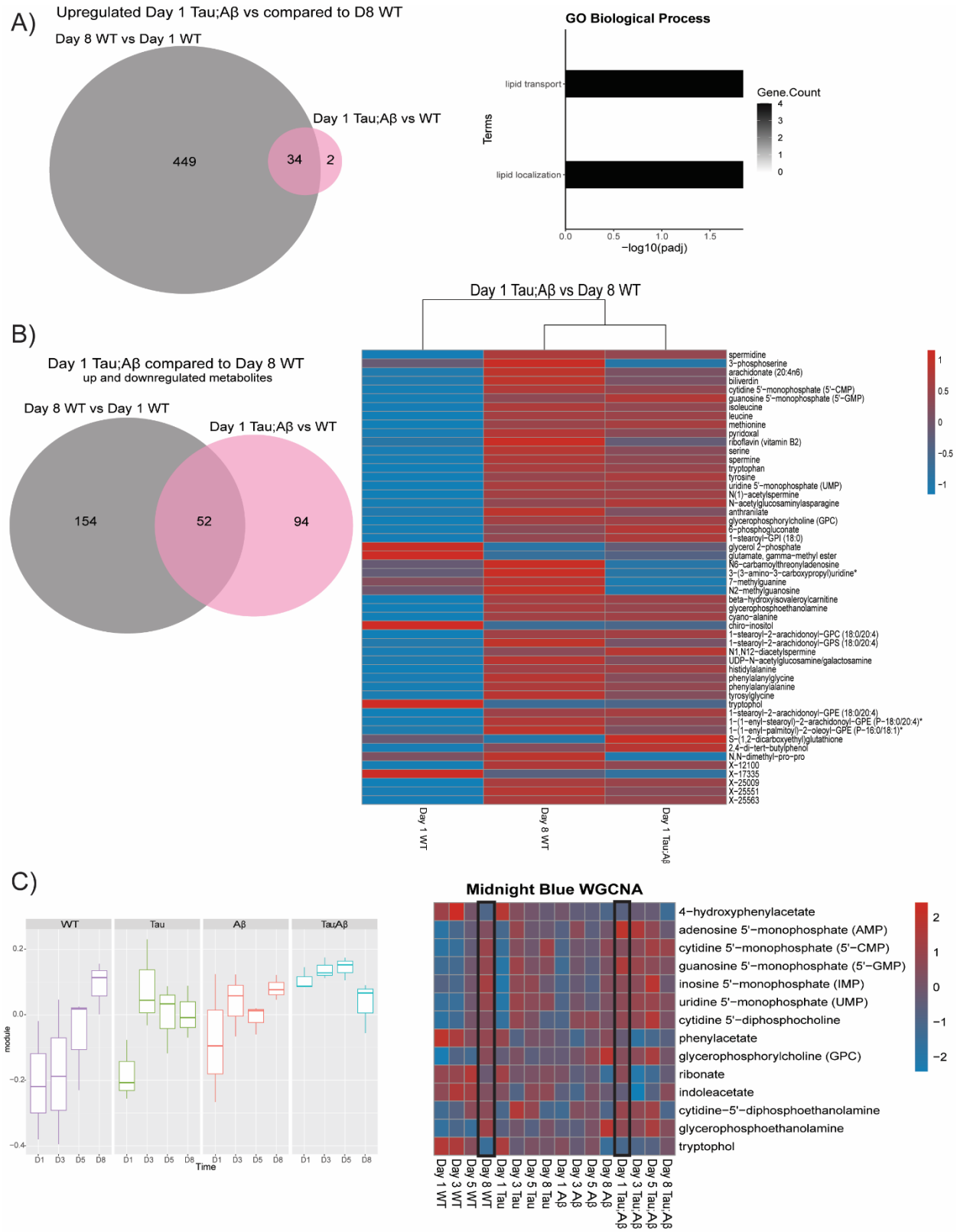
A)
Upregulated Day 1 Tau;Aβ vs compared to D8 WT
Day 8 WT vs Day 1 WT
Day 1 Tau;Aβ vs WT
449
34
2
GO Biological Process
lipid transport
lipid localization
Terms
Gene.Count
4
3
2
1
0
0.0
0.5
1.0
1.5
−log10(padj)
B)
Day 1 Tau;Aβ compared to Day 8 WT
up and downregulated metabolites
Day 8 WT vs Day 1 WT
Day 1 Tau;Aβ vs WT
154
52
94
Day 1 Tau;Aβ vs Day 8 WT
spermidine
3−phosphoserine
arachidonate (20:4n6)
biliverdin
cytidine 5'−monophosphate (5'−CMP)
guanosine 5'−monophosphate (5'−GMP)
isoleucine
leucine
methionine
pyridoxal
riboflavin (vitamin B2)
serine
spermine
tryptophan
tyrosine
uridine 5'−monophosphate (UMP)
N(1)−acetylspermine
N−acetylglucosaminylasparagine
anthranilate
glycerophosphorylcholine (GPC)
6−phosphogluconate
1−stearoyl−GPI (18:0)
glycerol 2−phosphate
glutamate, gamma−methyl ester
N6−carbamoylthreonyladenosine
3−(3−amino−3−carboxypropyl)uridine*
7−methylguanine
N2−methylguanosine
beta−hydroxyisovaleroylcarnitine
glycerophosphoethanolamine
cyano−alanine
chiro−inositol
1−stearoyl−2−arachidonoyl−GPC (18:0/20:4)
1−stearoyl−2−arachidonoyl−GPS (18:0/20:4)
N1,N12−diacetylspermine
UDP−N−acetylglucosamine/galactosamine
histidylalanine
phenylalanylglycine
phenylalanylalanine
tyrosylglycine
tryptophol
1−stearoyl−2−arachidonoyl−GPE (18:0/20:4)
1−(1−enyl−stearoyl)−2−arachidonoyl−GPE (P−18:0/20:4)*
1−(1−enyl−palmitoyl)−2−oleoyl−GPE (P−16:0/18:1)*
S−(1,2−dicarboxyethyl)glutathione
2,4−di−tert−butylphenol
N,N−dimethyl−pro−pro
X−12100
X−17335
X−25009
X−25551
X−25563
1
0.5
0
−0.5
−1
Day 1 WT
Day 8 WT
Day 1 Tau;Aβ
C)
WT
Tau
Aβ
Tau;Aβ
0.2
0.0
−0.2
−0.4
module
D1
D3
D5
D8
Time
Midnight Blue WGCNA
4−hydroxyphenylacetate
adenosine 5'−monophosphate (AMP)
cytidine 5'−monophosphate (5'−CMP)
guanosine 5'−monophosphate (5'−GMP)
inosine 5'−monophosphate (IMP)
uridine 5'−monophosphate (UMP)
cytidine 5'−diphosphocholine
phenylacetate
glycerophosphorylcholine (GPC)
ribonate
indoleacetate
cytidine−5'−diphosphoethanolamine
glycerophosphoethanolamine
tryptophol
2
1
0
−1
−2
Day 1 WT
Day 3 WT
Day 5 WT
Day 8 WT
Day 1 Tau
Day 3 Tau
Day 5 Tau
Day 8 Tau
Day 1 Aβ
Day 3 Aβ
Day 5 Aβ
Day 8 Aβ
Day 1 Tau;Aβ
Day 3 Tau;Aβ
Day 5 Tau;Aβ
Day 8 Tau;Aβ

Figure 6

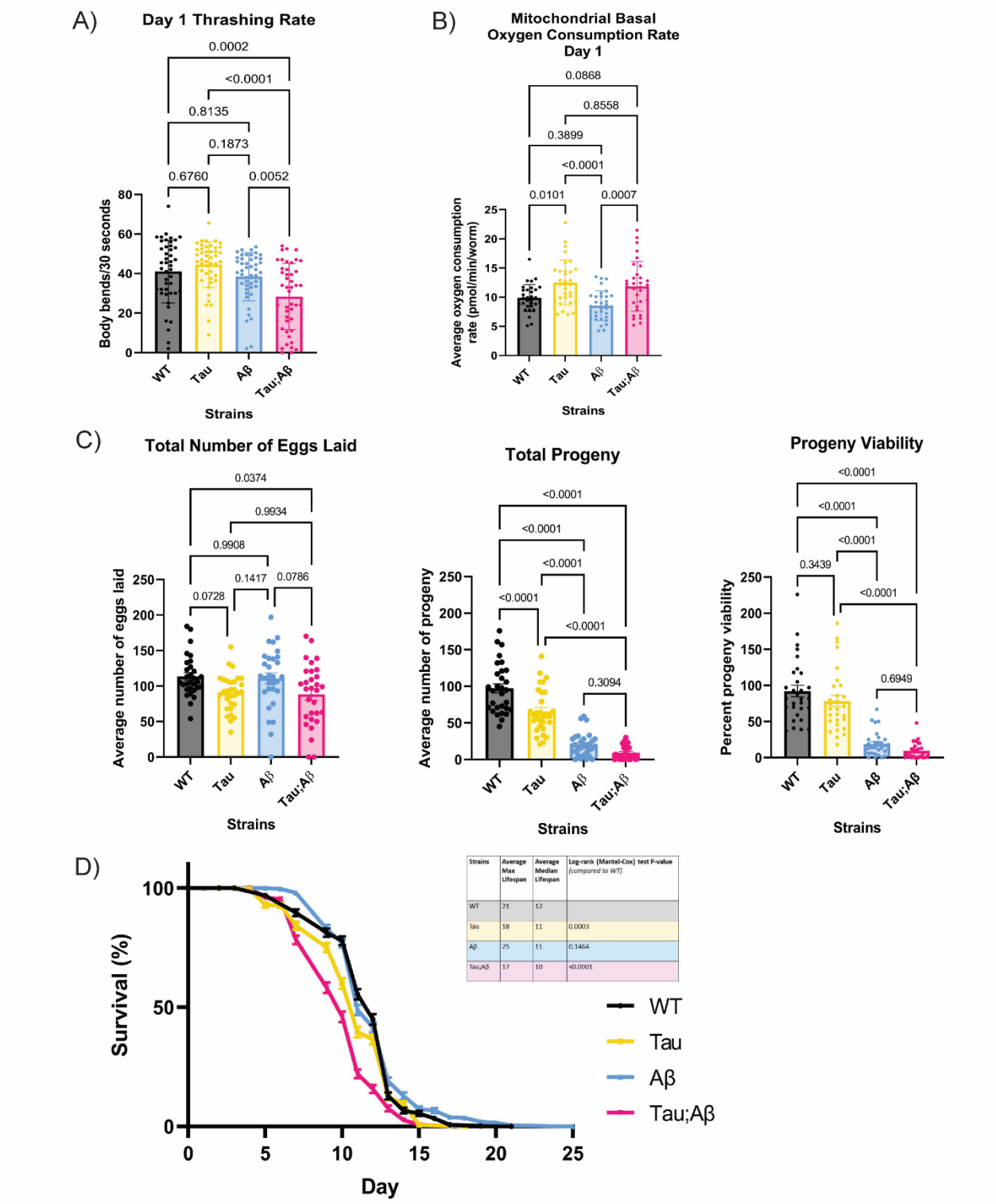

Strains	Average Max Lifespan	Average Median Lifespan	Log-rank (Mantel-Cox) test P-value *(compared to WT)*
WT	21	12	
Tau	18	11	0.0003
Aβ	25	11	0.1464
Tau;Aβ	17	10	<0.0001

Figure 7

A)

Tau vs WT	Aβ vs WT	Tau;Aβ vs WT
CELE_Y62H9A.6	vit-1	CELE_ZK180.6
CELE_D1054.10	CELE_ZC373.2	CELE_F10D11.6
CELE_ZK813.3	ttr-14	far-1
cbd-1	CELE_D1054.11	vit-1
perm-4	CELE_D1054.10	CELE_ZC373.2
	mup-4	col-184
	CELE_ZK813.3	tct-1
	CELE_Y62H9A.3	tbb-1
	vit-6	mup-4
	CELE_F48E3.4	ttr-14
	CELE_Y62H9A.6	CELE_D1054.11
	cht-3	F46H5.3
	perm-4	mua-3
	skpo-1	CELE_Y62H9A.5
	vit-2	grd-14
	vha-11	CELE_Y62H9A.3
	CELE_F55B11.2	pck-2
	cbd-1	cht-3
	efa-6	vha-13
	rpl-22	CELE_F48E3.4
	H28O16.1	vit-6
	CELE_Y47G6A.15	CELE_D1054.10
	let-805	vit-5
		fipr-21
		CELE_Y62H9A.6
		skpo-1
		rme-1
		car-1
		vit-2
		uba-1
		cbd-1
		perm-4
		rpl-4
		tba-1
		ant-1.1
		rpl-22
		pqn-22

B)

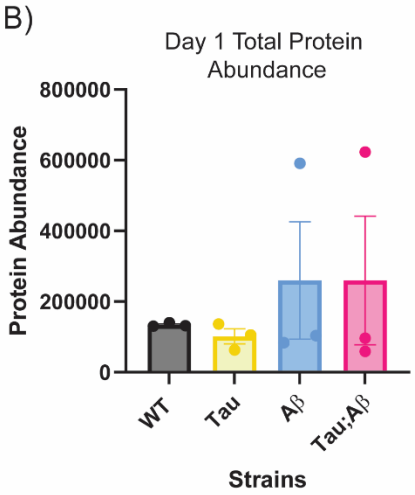

Supplementary Figure 1

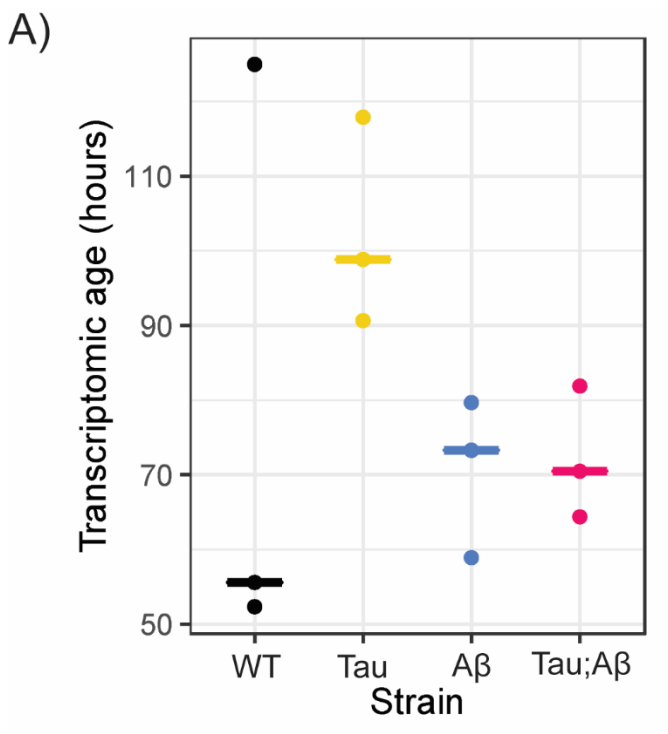

Supplementary Figure 2

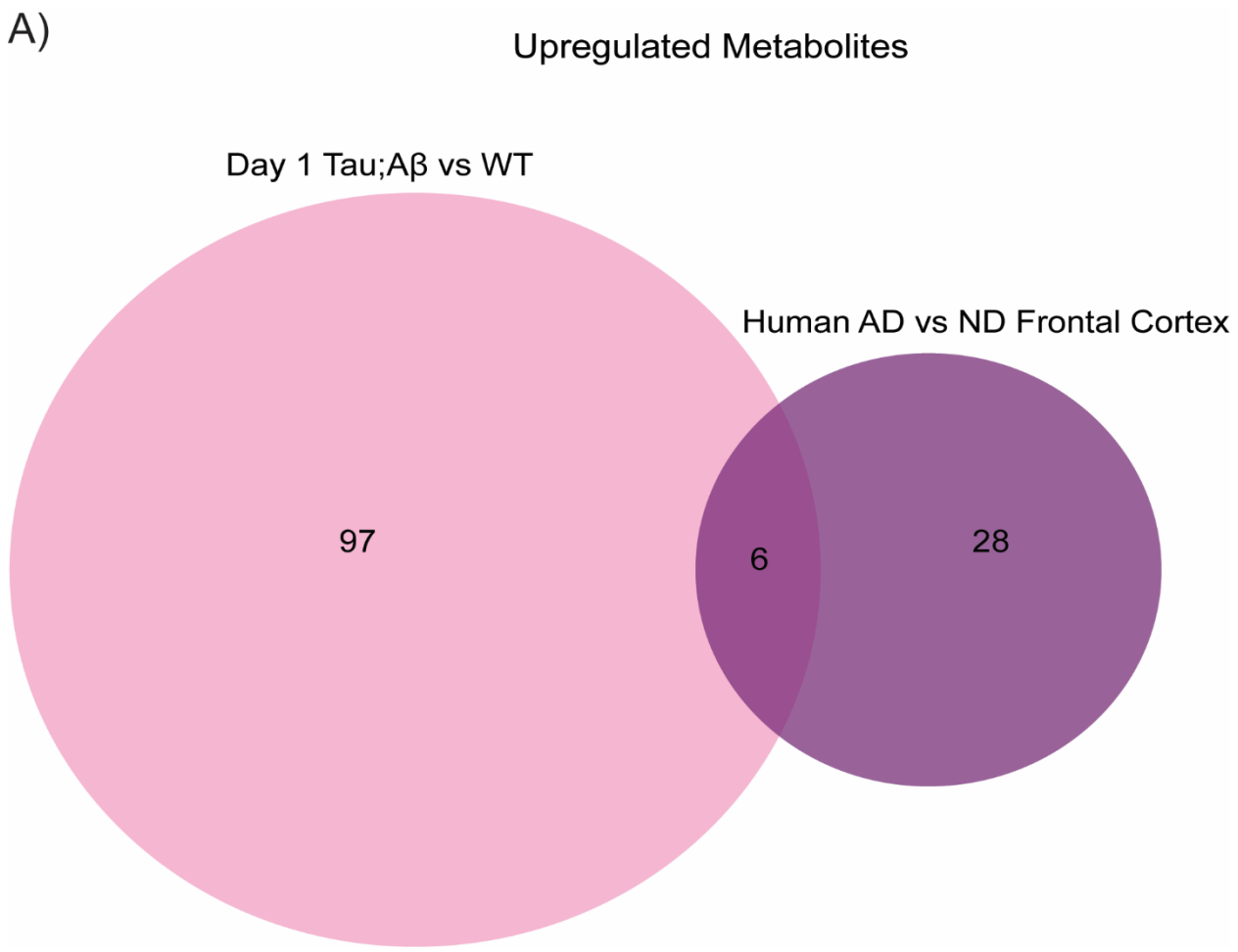

Supplementary Figure 3

A)

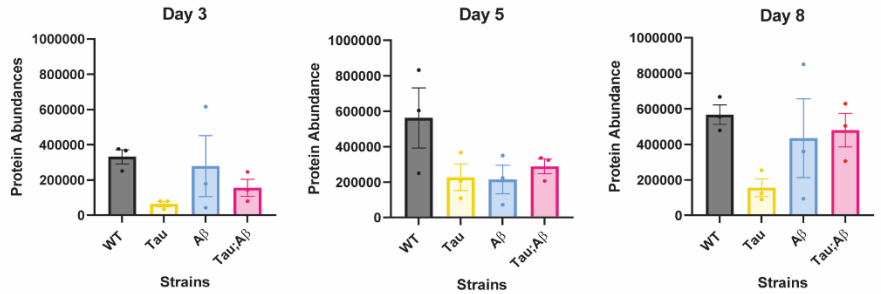

B)

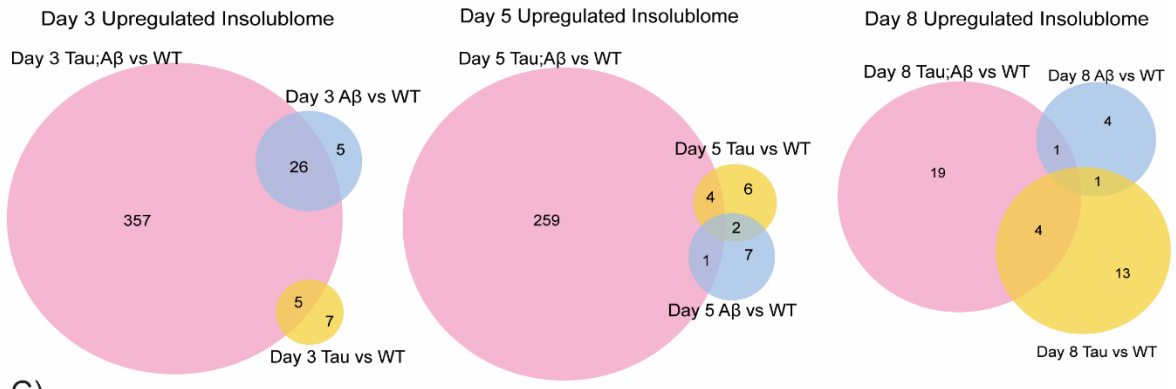

C)

Strain Comparison	Pathway Source	Term	-Log10(p-adj)	Gene Count	Proteins
Day 3 Tau;Aβ vs WT	WP	Cytoplasmic ribosomal proteins	1.392401	31	RPL-30,RPS-12,RPS-1,RPS-20,RPS-10,RPS-3,RPS-18,RPL-10,RPL-24.1,RPS-17,RPL-16,RPS-6,RPS-16,RPS-9,RPS-2,RPL-14,RPL-11.1,RPL-27,RPL-18,RPL-17,RPS-8,RPL-4,RPS-0,RPL-25.1,RPL-9,RPL-22,RPL-7A,RPS-4,RPL-5,RPL-6,RPL-3
Day 5 Tau;Aβ vs WT	GO:CC	Ribosome	1.422177869	25	RPL-17,RPS-5,RPS-19,RPS-7,RPS-12,RPS-1,RPS-3,RPL-16,RPL-9,RPS-8,RPS-6,RPL-7,RPS-16,RPL-5,RPL-12,RPL-36,RPL-22,RACK-1,RPS-9,RPL-4,RPS-2,RPL-19,RPS-4,RPS-0,RPL-6

D)

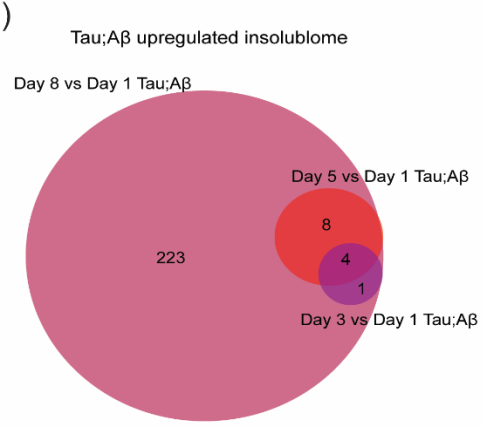

E)

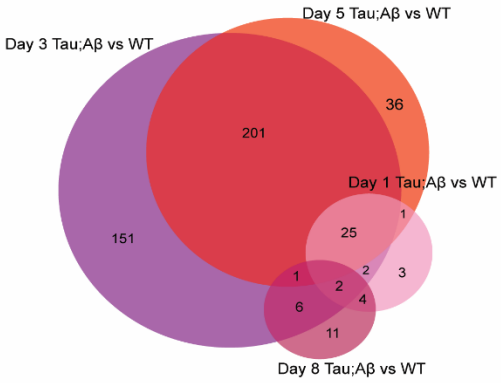

Supplementary Figure 4

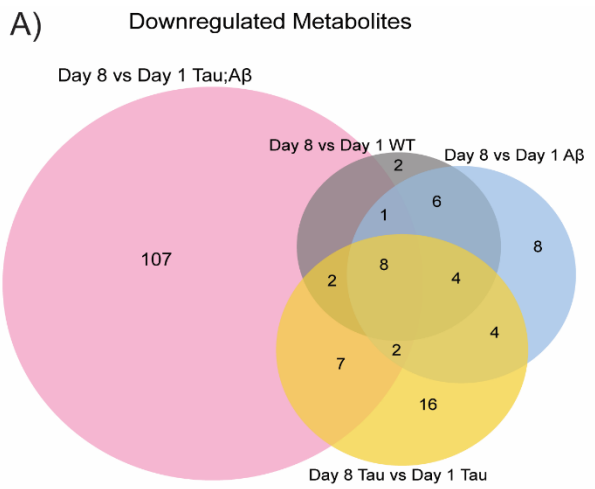

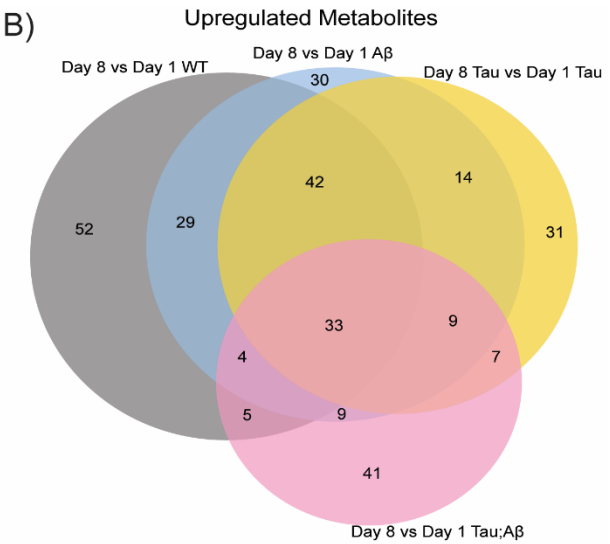

C)

Strain Comparison	# upregulated metabolites (q≤0.05)	# downregulated metabolites (q≤0.05)
Day 3 Tau vs WT	0	3
Day 3 Aβ vs WT	0	0
Day 3 Tau;Aβ vs WT	2	2
Day 5 Tau vs WT	0	2
Day 5 Aβ vs WT	0	0
Day 5 Tau;Aβ vs WT	23	18
Day 8 Tau vs WT	0	5
Day 8 Aβ vs WT	0	0
Day 8 Tau;Aβ vs WT	6	1

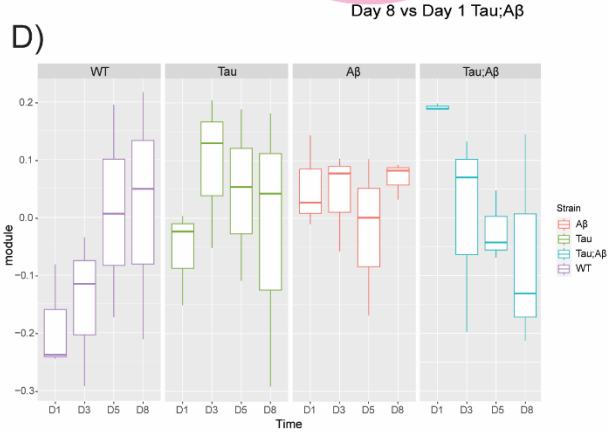

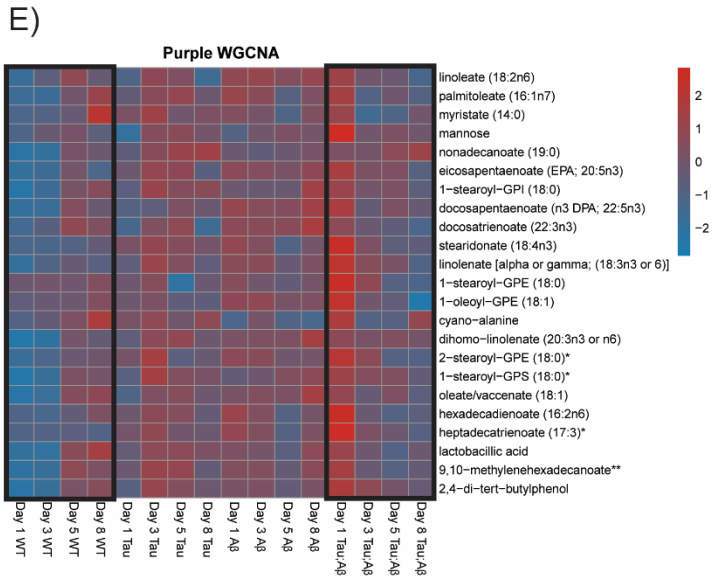

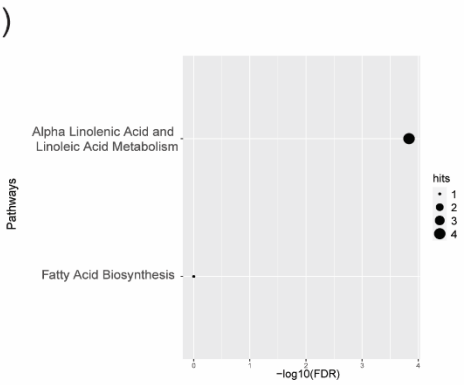

Supplementary Figure 5